small science
www.small-science-journal.com

Hybrid-Filler Stretchable Conductive Composites: From Fabrication to Application

Guolin Yun, Shi-Yang Tang, Hongda Lu, Shiwu Zhang, Michael D. Dickey,* and Weihua Li**

Stretchable conductive composites (SCCs) are generally elastomer matrices filled with conductive fillers. They combine the conductivity of metals and carbon materials with the flexibility of polymers, which are attractive properties for applications such as stretchable electronics, wearable devices, and flexible sensors. Most conventional conductive composites that are filled with only one type of conductive filler face issues in mechanical and electrical properties. Recently, some studies introduced secondary fillers to create hybrid-filler SCCs to solve these problems. The secondary fillers produce a synergistic effect with the primary fillers to enhance the electrical conductivity of the composites. They also improve the thermal conductivity and mechanical properties or impart composites with special functions like catalysis and self-healing. Herein, the fabrication methods, stretchability enhancement strategies, and piezoresistivity of SCCs are analyzed, and their latest applications in stretchable electronics are introduced. Finally, the challenges and prospects of their development are discussed.

1. Introduction

A conductive composite is a conductive material composed of conductive fillers in a nonconductive matrix. Among them, stretchable conductive composites (SCCs) generally consist of conductive fillers dispersed in elastomer and thus have a much higher mechanical stretchability than rigid metal or carbon conductive materials. Due to the ability to preserve electrical conductivity under mechanical deformation, SCCs have shown attractive applications in stretchable devices such as soft robots and wearable electronics.[1]

Most SCCs are filled with only one type of conductive filler and are thus called single-filler composites. Single-filler SCCs inevitably suffer from limitations such as low mechanical strength, poor stretchability, uneven filler dispersion, insufficient conductivity, degradation caused by oxidation, and poor repeatability. To solve these problems, many recent studies have introduced secondary fillers to enhance the physical or chemical properties of composites.[2] These composites filled with multiple fillers are called hybrid-filler composites.

There are a variety of reasons as to why secondary fillers are attractive. Their main function in hybrid-filler SCCs is to enhance the electrical conductivity by dispersing or bridging the primary fillers or by producing a synergistic effect with them. For instance, filler aggregation is a major problem for conductive composites filled with carbon fillers such as carbon nanotubes (CNTs), graphene, and carbon black (CB), which not only ineffectively uses the filler but also reduces the mechanical strength and electrical conductivity of the composites.[3] There are two main ways to solve this problem by introducing secondary fillers. One method is to use conductive polymers (CPs) (e.g., polyaniline) or dispersants (e.g., polyvinylcarbazole-based compatibilizer, β-cyclodextrin, and silane) as secondary fillers to improve the interface interaction between the carbon fillers and the matrix, thereby more uniformly dispersing them in the matrix.[4] Another method is to add secondary conductive fillers like metal nanoparticles (NPs) or other carbon fillers with different geometric shapes to achieve dispersion by breaking up filler aggregates during mixing.[5] The homogeneous dispersion of the main fillers can generally reduce its percolation threshold and enhance the electrical conductivity and mechanical strength of the composite.[4a,b,6] In addition, conductive secondary fillers can also fill

Dr. G. Yun, H. Lu, Prof. W. Li
School of Mechanical, Materials, Mechatronic and Biomedical Engineering
University of Wollongong
Wollongong, NSW 2522, Australia
E-mail: weihuali@uow.edu.au

Dr. S.-Y. Tang
Department of Electronic, Electrical and Systems Engineering
University of Birmingham
Edgbaston, Birmingham B15 2TT, UK
E-mail: S.Tang@bham.ac.UK

Prof. S. Zhang
Key Laboratory of Precision Scientific Instrumentation of Anhui Higher Education Institutes
Department of Precision Machinery and Instrumentation
University of Science and Technology of China
Hefei, Anhui 230027, China

Prof. M. D. Dickey
Department of Chemical and Biomolecular Engineering
North Carolina State University
Raleigh, NC 27695, USA
E-mail: mddickey@ncsu.edu

The ORCID identification number(s) for the author(s) of this article can be found under https://doi.org/10.1002/smsc.202000080.

DOI: 10.1002/smsc.202000080

the voids between the primary fillers as conductive bridges, which can reduce the contact resistance and improve the density of the conductive percolation network.[7] Using chemical reduction, previous studies have also grown or plated highly conductive secondary fillers like gold and silver on the main fillers to increase their conductivity.[8]

In addition, secondary fillers can also improve the thermal conductivity and mechanical properties or impart composites with special functions. Secondary fillers with high thermal conductivity such as metals and CNTs can be used to enhance the thermal conductivity of composites.[9] Using electrically conductive secondary fillers can improve both the electrical and thermal conductivities.[7b,10] Another important role of secondary fillers is to enhance the mechanical properties of composites, including Young's modulus,[11] storage modulus,[4b,12] tensile strength[4a,5d,13] shear strength,[14] impact toughness,[9a,15] tensile limit,[16] thermal stability,[17] and wear resistance.[18] Furthermore, single-filler conductive composites usually have limited functionality because fillers are only used for electrical conduction. In contrast, by selectively combining conductive and functional fillers, hybrid-filler composites can achieve different functions on demand while maintaining electrical conductivity. Using functional fillers, various conductive composites with unconventional functionalities have been developed in recent years, such as electroluminescent composites,[19] magnetically actuated composites filled with ferromagnetic particles,[20] self-healing composites filled with liquid metals (LMs),[7a,21] antioxidant composites filled with gold-plated fillers,[22] antibacterial composites filled with silver flakes,[23] composite catalysts,[24] and beyond.

Due to their excellent physical properties and diverse functions, hybrid-filler SCCs are increasingly used in the field of stretchable electronics. Many studies focus on their stretchability and response of electrical conductivity to strain.[1c,25] High stretchability allows the composite to withstand greater deformation, which can expand its fields of application. Using intrinsically stretchable fillers such as LMs or CPs is the easiest method to obtain highly stretchable SCCs.[1b,7a,26] Designing a stretchable microscopic filler network or a stretchable macroscopic geometry is the main method to enhance stretchability.[2a,25b,27] In contrast, the way the conductivity of SCCs changes in response to strain directly determines the role of the composites in electronic devices.[28] For example, a composite with a stable resistance under strain can be used as an electrode or interconnect, whereas a composite whose resistance changes during deformation is well suited for sensing strain. Therefore, it is necessary to understand the mechanism of the conductivity change of SCCs with respect to strain via simulations and experiments.

Starting with the combination of different types of fillers and matrices (**Figure 1**A), this Review details the fabrication methods (Figure 1B) and stretchability enhancement strategies (Figure 1C) of SCCs. We will particularly focus on hybrid-filler composites. Aspects of composites with single fillers have been reviewed in other studies.[1c,25] According to the distribution of fillers in the matrix, the preparation methods are divided into two categories: homogeneous mixing and heterogeneous assembly.[1c] Stretchability enhancement strategies include using intrinsically stretchable fillers and designing the stretchable filler networks and geometric macrostructures. Subsequently, we summarize the common numerical models and theories used to describe the electrical conductivity of composites and analyze the piezoresistive types of conductive composites. Here, the term piezoresistivity refers to the change in the electrical resistivity of a composite in response to mechanical strain. Focusing on different piezoresistive properties, the last chapter introduces the latest applications of hybrid-filler SCCs in electrodes, sensors, functional actuators, and other stretchable electronic devices (Figure 1D). Finally, we evaluate the advantages and disadvantages of the SCCs and outline challenges for future research.

We define the key terminologies used in this Review. 1) Positive piezoresistivity: the SCC's electrical resistivity increases with increasing strain, that is, the resistivity increases upon stretching (positive strain) and decreases upon compression (negative strain). 2) Negative piezoresistivity: the electrical resistivity of the SCC decreases upon stretching and increases upon compression. 3) Gauge factor (GF): the ratio of normalized electrical resistance change ($\Delta R/R_0$, where ΔR is the resistance change and R_0 is the initial resistance) to strain (ε), which can be calculated as $\mathrm{GF} = (\Delta R/R_0)/\varepsilon$.

The key features of representative hybrid-filler SCCs are shown in **Table 1**, including the raw materials, fabrication methods, stretchability enhancement strategies, mechanical stretchability, electrical conductivity, piezoresistive properties, and applications. We selected SCCs that contain as many of these key features as possible. Most of them come from research in the last three years to show the latest development direction of hybrid-filler SCCs. We hope that this Review can provide a reference for the future studies and inspire new applications of SCCs.

2. Fabrication

The electrical properties of SCCs, such as electrical conductivity and piezoresistivity, are generally determined by the composition and concentration of conductive fillers, whereas the elastic matrix mainly affects their mechanical properties like modulus, elasticity, and strain at failure. In addition, SCCs with different processing methods may also exhibit disparate electrical and mechanical properties. This section will introduce the commonly used conductive fillers, matrices and fabrication methods of SCCs.

2.1. Materials

The electrical properties of SCCs mainly depend on the type, shape, size, and concentration of the fillers.[25a] Depending on the type, conductive fillers can be divided into metals, metal oxides, carbon-based fillers, and CPs. They have four main morphologies: particle, flake, wire, and liquid (Figure 1A).

2.1.1. Metal Fillers

Metal fillers have the highest electrical conductivity among all types of fillers and are therefore widely used in SCCs.[29] Sometimes their oxides are used instead to improve the environmental and chemical stability of composites. Their shapes, size, dispersion, and alignment directly affect the electrical conductivity and the strain response of SCCs. The conductivity of SCCs

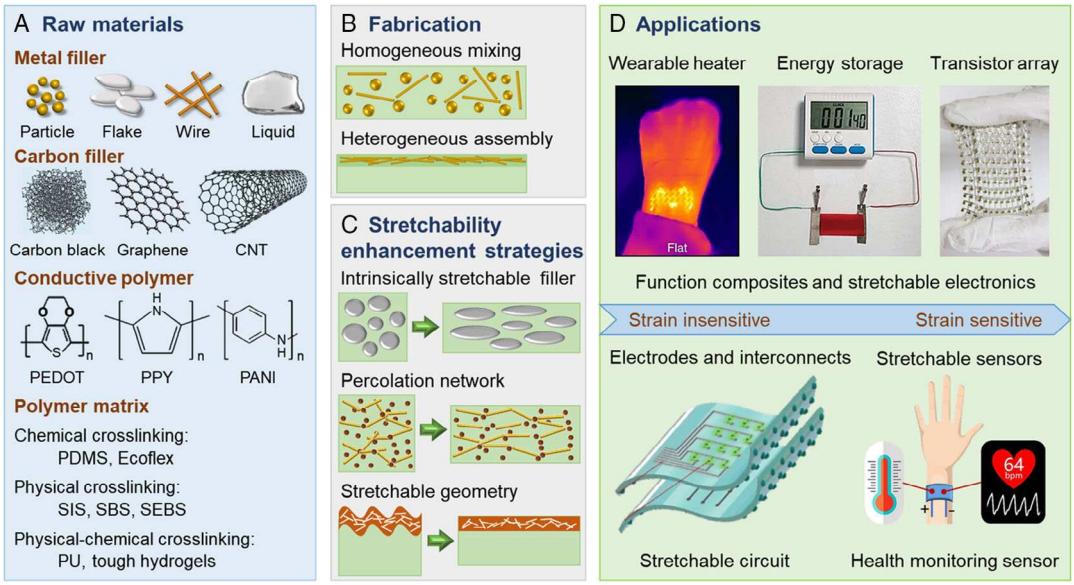

Figure 1. An introduction of SCCs: raw materials, fabrication methods, stretchability enhancement strategies, and their applications in stretchable electronics. A) Common conductive fillers and matrices of SCCs. B) Two types of fabrication methods of SCCs. C) Three types of stretchable design strategies of SCCs. D) Applications of SCCs corresponding to different strain sensitivities. Wearable heater: Adapted with permission.[22] Copyright 2018, Springer Nature. Energy storage composite: Reproduced with permission.[21] Copyright 2018, Wiley-VCH. Transistor array: Adapted under the terms of the CC-BY 4.0 license.[34] Copyright 2015, The Authors, published by Springer Nature. Stretchable circuit: Adapted under the terms of the CC-BY 4.0 license.[100] Copyright 2019, The Authors, published by Wiley-VCH.

filled with metal particles is generally low and requires high loading to achieve percolation. Such composites are extremely sensitive to mechanical deformation due to the low aspect ratio of the fillers.[30] When the composite is stretched, the metal particles will separate from each other and thus the conductivity decreases drastically (**Figure 2**A).[31–33] In contrast, the electrical conductivity of composites filled with fillers of high aspect ratio generally has low strain sensitivity. Flake-shaped fillers can overlap like pages in a book. They can slide horizontally and keep in contact with each other during stretching to maintain high conductivity (Figure 2B).[34–36] Metal wires with high aspect ratio can form a continuous network structure in the elastic matrix to create highly percolated conduction paths. This allows them to preserve electrical contact during large deformation and thus effectively improve the conductivity and stretchability of the SCCs (Figure 2C).[37]

However, most metal fillers have poor mechanical flexibility, which will reduce the tensile fracture strain of the SCCs. One approach to solve this problem is to introduce stretchable LM fillers. Here, the LM refers to gallium-based alloys such as EGaIn, a mixture of 75% gallium and 25% indium. It is liquid at room temperature and has high electrical/thermal conductivities and high deformability.[38] In theory, LM can be stretched indefinitely while maintaining constant metal conductivity. This extraordinary property helps improve the stretchability of SCCs.[39] During deformation, stretchable fillers such as LM can deform along with the matrix to preserve the filler conductive network (Figure 2D).[40] Therefore, adding LM as the secondary filler to the SCC can significantly reduce the strain sensitivity of composites during stretching.[21,36,41] However, this also leads to the fact that LM-filled single-filler SCCs often show low strain sensitivity and are not suitable for use in sensors. In addition, the high LM volume fraction is needed for percolation in single-filler SCCs, which may lead to leakage of LM under large mechanical loads. Furthermore, the gallium-based LM will rapidly form a thin surface gallium oxide layer in the air, which may hinder the charge transfer in the composite to a certain extent and reduce its electrical conductivity.[42]

2.1.2. Carbon Fillers

Carbon-based fillers appear to be the most popular conductive fillers in recent years. Such fillers include CB, carbon fiber (CF), CNTs, and graphene (Figure 1A).[43] SCCs with carbon fillers have been reviewed in the study by Sun et al. in detail.[44] The shape and aspect ratio of carbon fillers are key factors affecting the strain response of conductive composites. Granular CB is commonly used as the conductive filler due to the controllable particle size, relatively low cost, and high conductivity.[45] But it has the same disadvantage as metal particles, that is, the CB-filled composite shows a sharp ascent in resistance during stretching.[32,46] CF is a high-strength micrometer-sized fiber material that has good resistance to corrosion and fatigue.[47] But its electrical conductivity is relatively low compared with CB and CNTs, so it is mainly used to enhance the mechanical strength of composites. CNTs have not only excellent mechanical properties, but also higher electrical and thermal conductivity than CFs. High aspect ratio (up to several thousands) enables CNTs to form a percolated conductive network, which makes it an excellent conductive filler.[48] Graphene is a 2D honeycomb carbon nanomaterial with excellent mechanical strength,

Table 1. Key features of representative hybrid-filler SCCs.

Fillers[a)]	Matrix	Fabrication methods	Stretchability enhancement strategy	Fracture strain[b)]	Electrical conductivity	Piezoresistivity[c)]	Stretchable application	Ref.
AgNP NiNP	PDMS	Direct mixing	Percolation network	225%	0.574 Ω sq^{-1}	4.5 Ω sq^{-1}@225%	EMI-shielding film	[31]
AgNP graphene	PVDF	Solution mixing hot rolling	Percolation network	50%	301 200 S m^{-1}	32 280 S m^{-1}@35%	Electrode	[168]
Flower-shaped AgNP trichlorosilane	PU	Solution mixing wet spinning	Flower-shaped filler	180%	1.46 MS m^{-1}	63 kS m^{-1}@100%	Water- and oil-resistant conductive fabric	[88]
AgNW AgNP	SBS	Wet spinning chemical reduction	Percolation network	900%	245 000 S m^{-1}	$\sigma/\sigma_0 = 4.4\%$@100%	Joint motion sensor sign language recognition glove	[74]
AgNW graphene	PDMS	Spin coating	Percolation network	100%	33 Ω sq^{-1}	$R/R_0 = 1$@66% $R/R_0 = 1.13$@100% strain insensitive	Electrode	[148]
AgNW CF PU foam	PDMS	Matrix infiltration	Porous structure	140% WR[d)]	1037 S m^{-1}	596 S m^{-1}@140%	Electrode	[96]
AgNF AgNW	PDMS	Electrospinning Electrospray	Percolation network	90% WR	1.03 Ω sq^{-1}	$R/R_0 = 1.28$@90% $R/R_0 = 41$@100%	Electrode	[7e]
Gold-plated AgNW	SBS	Electroless plating solution mixing	Percolation network hot rolling	266% 840% after hot rolling	4.185 MS m^{-1}	0.4 MS m^{-1}@266%	Wearable and implantable bioelectronic patch	[22]
Ag flake Ag nanocrystal	PDMS	Direct mixing hot welding	Percolation network	80%	234 520 S m^{-1}	41 300 S m^{-1}@80%	Muscle motion sensor joint motion sensor	[35]
Ag flake AgNP fluorosurfactant	Liquid fluorine rubber	Direct mixing	Percolation network	400%	616 800 S m^{-1}	93 500 S m^{-1}@400%	Electrical interconnection	[8d]
Ag flake fluorosurfactant	Fluorine rubber	Solution mixing	Percolation network	215%	73 800 S m^{-1}	18 200 S m^{-1}@215%	Electrical interconnection	[34]
Sulfur crosslinker AgNW aerogel	*N*-isopropylacrylamide	Unidirectional freezing matrix infiltration	Porous structure	1230%	9300 S m^{-1}	$R/R_0 = 1.2$@100% $R/R_0 = 2.3$@500%		[118]
Ag−poly(vinylpyrrolidone) submicrometer fiber	PET	Dry spinning hot welding	Mesh structure	30% WR	7 Ω sq^{-1}	$R/R_0 = 1.12$@30%	Transparent heating film	[120]
Cu−Ag core−shell structure NW	PU	Hot welding	Percolation network	80%	35 Ω sq^{-1}	$R/R_0 = 23$@80%	Transparent heater	[94]
Silver-plated CuNW	Ecoflex dragon Skin	Electroless plating matrix infiltration	Serpentine structure	350%	122 000 S m^{-1}	$R/R_0 = 4$@150%	Electrical interconnection	[8c]
AuNW AgNW	PDMS	Drip casting	Percolation network	70%		$R/R_0 = 2.4$@60% $R/R_0 = 4.5$@70%	Muscle motion sensor	[56]
AuNW gold coating	SEBS	Solution mixing dry spinning	Prestretch	380%	6210 S m^{-1}	46 120 S m^{-1}@380% Negative	Electrical interconnection	[92]
Gold-plated TiO_2NW	PDMS	Electroless plating spin coating	Percolation network	150%	0.63 Ω sq^{-1}	7 Ω sq^{-1}@100%	Electrode grid	[8b]
Ni particle CB	PDMS	Direct mixing	Spiky-shaped filler	−30% WR	2 MΩ·m	0.2 Ω·m@−30%		[58]
Metal nanotrough graphene	PDMS	Electrospinning chemical deposition	Percolation network	80%	1 Ω sq^{-1}	$R/R_0 = 1.1$@70% $R/R_0 = 1.3$@80%	Electrode	[77]
Acrylate-functionalized EGaIn particle	2-hydroxyethyl acrylate	Drip casting	Intrinsically stretchable	744%	After the rupture of LM droplets: 400 S m^{-1}	$R/R_0 = 1$@300% 20 000 S m^{-1}@700% Negative	Heating film	[26a]

Table 1. Continued.

Fillers[a)]	Matrix	Fabrication methods	Stretchability enhancement strategy	Fracture strain[b)]	Electrical conductivity	Piezoresistivity[c)]	Stretchable application	Ref.
EGaIn AgNP	PDMS	Ink printing	Intrinsically stretchable	110%	4.85 MS m^{-1}	$R/R_0 = 1.8$@80% linear increase	Electrical interconnection	[41]
EGaIn Ag flake	Poly(ethylene-co-vinyl acetate)	Solution mixing	Intrinsically stretchable percolation network	1000%	800 000 S m^{-1}	$R/R_0 = 4.7$@700% $R/R_0 = 6.3$@900%	Capacitive sensor	[36]
EGaIn FeMP/NiMP	PDMS	Direct mixing	Percolation network	Fe: 20% Ni: 32.5 %	Fe: 40 kΩ·m Ni: 70 kΩ·m	Fe: 0.2 kΩ·m@±18% Ni: 0.015 Ω·m @ ± 10% Special	Magnetic/pressure control signal amplifier intelligent heating film	[103]
EGaIn Fe particle	Ecoflex	Ink printing	Intrinsically stretchable	Depends on the substrate	1.53 MS m^{-1}	$R/R_0 = 18$@300%	Recyclable printed circuit	[100]
EGaIn Ni flake	CPU	Solution mixing	Intrinsically stretchable percolation network	700%	247 900 S m^{-1}	$R/R_0 = 18.7$@700%	Energy-storage material	[21]
EGaIn graphene sheet	PDMS	Solution mixing Press rolling	Intrinsically stretchable	80%	850 S m^{-1}	Lateral compression $R/R_0 = 0.995$ @−33.7 kPa	Patterned electrical interconnect	[7a]
Liquid gallium gold film	PDMS	Physical vapor deposition	Serpentine structure	400%	0.5 Ω sq^{-1}	$R/R_0 = 1.9$@80%	Wearable sensor/ heater electrode	[117]
SWCNT−MWCNT	Thermoplastic polyurethane	Electrospinning ultrasonic adsorption	Percolation network	1250%	1300 S m^{-1}	$R/R_0 = 2.2$@100% $R/R_0 = 5.6$@200%	Joint motion sensor	[11b]
CNT CB	PDMS	Solution mixing	Percolation network	300%	0.25 S m^{-1}	$R/R_0 = 14.1$@300%	Joint motion sensor	[7d]
CNT CB	Ecoflex	Solution mixing	Percolation network fiber filler alignment	200% WR	150 Ω sq^{-1}	$R/R_0 = 1.4$@200%	Current collector for rechargeable lithium-ion battery	[65]
CNT graphene	Polyimide	Solution mixing matrix infiltration	Porous structure percolation network	−9.62% (1 MPa) WR	0.025 S m^{-1}	$R/R_0 = 0.11$@−9.62%	Pressure sensor	[7b]
CNT graphene	Liquid silicone rubber	Direct mixing fermentation foaming	Porous structure percolation network	96%		$R/R_0 = 0.926$@90% Negative		[16a]
CNT graphene	PDMS	Chemical vapor deposition	Percolation network	20%	≈4 kΩ sq^{-1}	$R/R_0 = 1.03$@9% Linear increase	Strain sensor	[75]
CNT graphene aerogel		Freeze drying	Porous structure	−90% WR	13 S m^{-1}	83 S m^{-1}@−90%	Strain sensor	[71]
CNT graphene foam	PDMS	Chemical vapor deposition matrix infiltration	Porous structure percolation network	>100%		$R/R_0 = 6.16$@85%	Muscle motion sensor	[97]
CNT graphite MP	Paper−polypropylene double-layer film	Solution mixing ink printing			99 Ω sq^{-1}	Indirect compressive strain by bending the film $R/R_0 = 0.94$@−0.54%	Light/thermal actuator strain/light/ humidity sensor	[138]
CNT PANI	SIS	Solution mixing	Percolation network	7% WR	≈100 S m^{-1}	$R/R_0 = 1.3$@7%	Strain sensor	[67]
CNT PANI	PET	Interfacial polymerization self-assembly	Percolation network	> 450%	295 Ω sq^{-1}	$R/R_0 = 0.45$@100% $R/R_0 = 0.45$@450% Negative	Transparent electrode	[145]

Table 1. Continued.

Fillers[a)]	Matrix	Fabrication methods	Stretchability enhancement strategy	Fracture strain[b)]	Electrical conductivity	Piezoresistivity[c)]	Stretchable application	Ref.
CNT PANI particle	PDMS	Direct mixing	Percolation network		0.0092 S m^{-1}	$R/R_0 = 1.5$@−10% Negative	Pressure sensor	[63]
CNT AgNW	Polyacrylate	Solution mixing cold welding	Prestretch percolation network	580%	7.1 Ω sq^{-1}	Uniaxial stretching $R/R_0 = 1.42$@580% equibiaxial stretching $R/R_0 = 2$@200%	Electrode	[95]
CNT AgNW	Ecoflex	Matrix infiltration plasma welding	Percolation network	> 520%	18 Ω sq^{-1}	$R/R_0 = 11$@320% $R/R_0 = 30$@460%	Electrical interconnection	[69]
CNT Ag nanobelt	PU	Wet spinning		> 15%	100 000 S m^{-1}	$R/R_0 = 300$@10% Linear increase	Electrode strain sensor	[89]
CNT iron oxide polypyrrole	Elastin peptide cryogel	Physical crosslink	Porous structure percolation network	−97.50%	≈55 S m^{-1}	1470 S m^{-1}@−70% 5010 S m^{-1}@−90%	Pressure sensor magnetic control actuator	[20]
CNT tetrapod zinc oxide	PDMS	Matrix infiltration	Percolation network	−30% 60%	130 S m^{-1}	130 S m^{-1}@−13% strain insensitive	Electrode	[11a]
CNT SiNP	Ecoflex	Direct mixing 3D printing	Fabric structure	−60% WR		$R/R_0 = -0.096$ kPa^{-1} Negative	Highly sensitive pressure sensor	[142]
CB branched carbon nanostructure	PU	Melt mixing	Percolation network	100% WR	70 Ω·m	$R/R_0 = 100$@100%	Strain sensor	[32]
Graphene Ca^{2+}	Silk fibroin	Solution mixing screen printing	Intrinsically stretchable	110%		$R/R_0 = 9.5$@70%	Strain/humidity/ temperature sensor	[83]
Graphene CB	PDMS	Solution mixing screen printing		20%	780 S m^{-1}	$R/R_0 = 12$@130%	Electrode	[84]
Graphene sheet Calcium hydroxide nanospherulite	Polyacrylamide	Solution mixing in situ polymerization	Porous structure	5800%	5.18 Ω·m	$R/R_0 = 3.3$@500%	Strain sensor	[5a]
Graphene−Fe_3O_4 hybrid sheet	PDMS	Direct mixing hot rolling				$R/R_0 = 870$@−22.9% Negative	Pressure sensor	[144]
Au−Ni coating graphene PU foam	PDMS	Electroless plating matrix infiltration	Porous structure percolation network	30% WR		$R/R_0 = 1.6$@30%	Electrical interconnection	[8a]
Carbon NF Graphene sheet	PDMS	Spin coating	Percolation network	50% WR		$R/R_0 = 2.65$@50% Linear increase	Joint motion sensor	[79]

[a)]SCCs are grouped according to the types of primary fillers, including solid metal fillers, LM fillers, and carbon fillers. [b)]Fracture strain refers to the ultimate tensile or compressive strain of a composite when it breaks. Positive values indicate stretching, and negative values indicate compression. Some composites do not provide fracture strain but give their working range instead. [c)]This column shows the resistance change of a composite under a specific strain and its piezoresistive properties. The Negative and Special represent Negative piezoresistivity and Special piezoresistivity, respectively. Unspecified composites are positive piezoresistive. [d)]WR: working range.

toughness, and electrical conductivity.[44b] These properties allow it to be used in the high-strength conductive composites. Unlike metal flake fillers, under large mechanical deformation, the carbon atom plane of graphene in the elastic matrix can bend and deform to avoid damage to the conductive network. Moreover, the concentration of CNT or graphene needed to form a conductive network in most SCCs is very low. When their volume fraction increases from 0.1% to 1%, the electrical conductivity of the composite can usually increase sharply by several orders of magnitude.[44b,49]

2.1.3. Conductive Polymer Fillers

In addition to metal and carbon fillers, CP fillers have also been widely used in SCCs due to their charge transport capability and excellent mechanical ductility. Commonly used CPs include, for example, polyaniline (PANI), polypyrrole (PPY), and poly(3,4-ethylenedioxythiophene):polystyrene sulfonate (PEDOT:PSS).[1b,26b,50] CPs can be easily processed into conductive fillers of different shapes such as particles and fibers, thereby giving the SCCs different strain responses. However, it is difficult for CPs

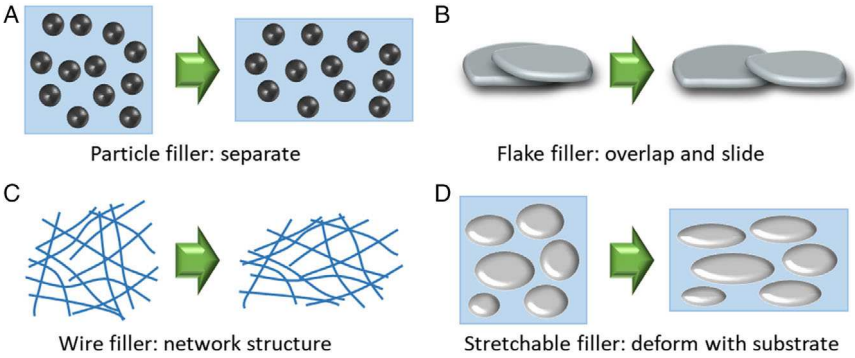

Figure 2. The strain response of the electrical conductivity of SCCs with different filler shapes. A) Particle filler, B) flake filler, C) wire filler, and D) stretchable filler.

to achieve high conductivity and mechanical stretchability simultaneously. The homogeneous dispersion of CP fibers in the matrix is also a major challenge. Therefore, auxiliary fillers are usually used to improve the electrical and mechanical properties of SCCs using CP fillers.[51] For instance, adding CNTs significantly increased the conductivity and tensile strength of a conductive composite using PANI as the primary filler.[4a] As another example, ionic liquid was added to an elastic conductor filled with PEDOT:PSS to increase its fracture strain to 800%.[52] Naphthalene compatibilizer can offer better dispersion of PANI in composites.[53] In addition, CPs can also be used as the auxiliary filler to improve the electrical property of SCCs.[54]

2.1.4. Combination of Primary and Secondary Fillers

The primary and secondary fillers in hybrid-filler SCCs usually have different shapes or types. The combination of different fillers endows hybrid-filler composites superior performance than single-filler composites.

Most hybrid-filler SCCs are filled with fillers of different geometric characteristics. For example, LM or secondary fillers with a high aspect ratio are usually introduced into particle-filled SCCs to enhance their electrical conductivity.[41,55] These secondary fillers can also adjust the strain sensitivity of the composite.[32,36] Conversely, particulate secondary fillers (e.g., CBs and AgNPs) can also fill the gaps of primary fillers (e.g., CNTs and silver microplates) to reduce junction resistance and increase conductivity.[7d,8d] Some researchers have also bridged the primary fillers using small-sized metal nanowires (NWs) to achieve the same purpose.[7e,56]

In addition, many hybrid filler SCCs use secondary fillers with properties different from primary ones to compensate for their shortcomings. On the one hand, the electrical conductivity of carbon fillers is much lower than that of metals. They also aggregate easily and are difficult to disperse well in the matrix. Fortunately, both problems can be solved by adding auxiliary fillers such as metal NPs or dispersants to the composites.[4b,6,57] On the other hand, adding carbon or polymer secondary fillers to metal-filled SCCs is also a common method to enhance mechanical properties such as mechanical strength, stretchability, and cyclic load stability.[58,59]

Finally, hybrid filler composites can also achieve various functions by adding secondary fillers with special physical and chemical properties. For example, composites filled with iron or iron oxide particles can be manipulated by a magnetic field.[20,21] The LM secondary filler can maintain the conductivity of the composite under mechanical damage.[21] As another example, composites containing silver secondary fillers can be used as antibacterial materials.[23]

2.1.5. Elastomer Matrices

Generally, the elastic matrix is insulating and thus does not contribute directly to the electrical properties of the SCCs. It mainly affects the mechanical properties, such as Young's modulus, tensile strength, and fracture strain.[25a] Polymer matrices with lower Young's modulus usually have higher tensile limits.[60] There are two types of crosslinking used to form polymer networks: physical crosslinking and chemical crosslinking.[1c,25a] Silicones are the most commonly used chemically crosslinked elastomers. Their polymer chains are connected by covalent bonds to form stable mechanical structures. In contrast, the polymer chains of physically crosslinked elastomers are generally connected by weak interactions such as hydrogen bonds. This interaction is weaker than chemical covalent bonds and therefore generally leads to poor elasticity of the polymers. However, it can be reshaped under high temperature and pressure, showing good processability. Polyurethane (PU) and some other tough hydrogels have both physical and chemical crosslinking bonds.[61] These tough hydrogels with extremely high tensile limits are widely used in stretchable electronics. It should be noted that the type, geometry, and concentration of conductive fillers also affect the mechanical properties of the composites. For instance, increasing filler concentration usually leads to increased hardness and reduced mechanical stretchability. Therefore, it is necessary to comprehensively consider the effect of fillers and matrices in manufacturing SCCs.

2.2. Fabrication Methods

In addition to fillers and elastomers of SCCs, processing methods also play an important role in determining their electrical and mechanical properties, such as electrical conductivity, strain response, and tensile limit.[62] This section will introduce and compare common fabrication techniques for SCCs in recent research.

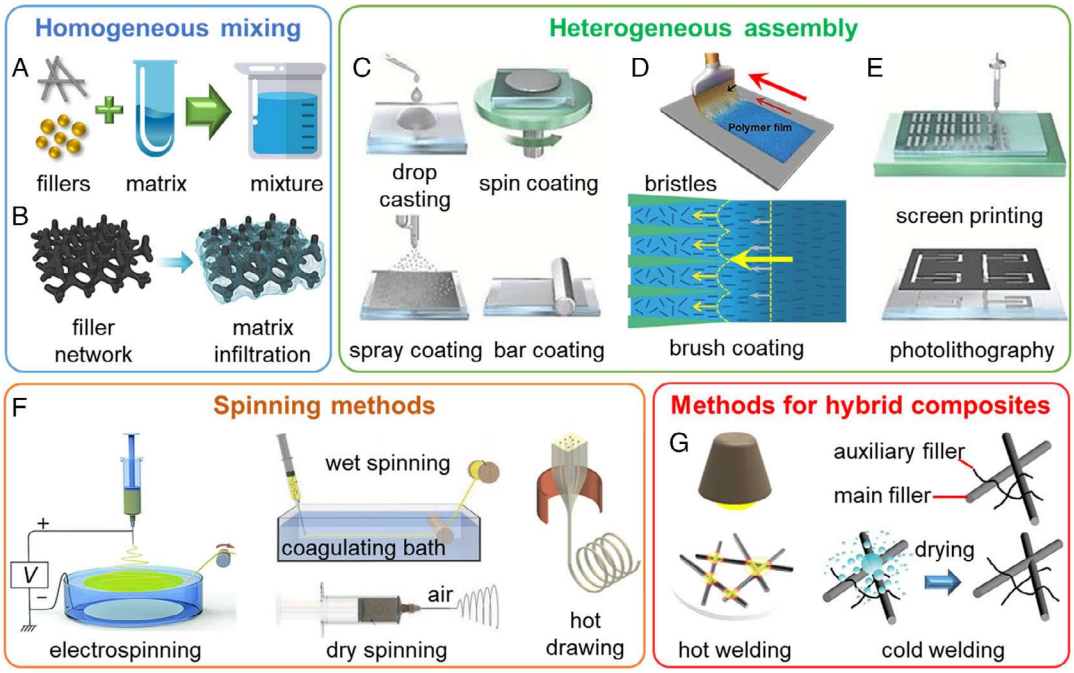

Figure 3. Fabrication methods of SCCs. A) Filler matrix mixing method. B) Matrix infiltration method: Adapted with permission.[167] Copyright 2017, Wiley-VCH. C) Drop casting, spin coating, spray coating, and bar coating: Reproduced with permission.[1c] Copyright 2019, Wiley-VCH. D) Brush coating: Adapted with permission.[82] Copyright 2017, Wiley-VCH. E) Screen printing and photolithography: Reproduced with permission.[1c] Copyright 2019, Wiley-VCH. F) Electrospinning, wet spinning, dry spinning, and hot drawing. Electrospinning: Adapted with permission.[11b] Copyright 2018, Royal Society of Chemistry. Wet spinning: Adapted with permission.[74] Copyright 2015, Wiley-VCH. Dry spinning: Adapted with permission.[92] Copyright 2018, Wiley-VCH. Hot drawing: Reproduced with permission.[40a] Copyright 2018, Wiley-VCH. G) Hot welding and cold welding. Hot welding: Reproduced with permission.[69] Copyright 2014, IOP Publishing. Cold welding: Adapted with permission.[95] Copyright 2019, Wiley-VCH.

2.2.1. Homogeneous Mixing Method

Mixing fillers and matrix homogeneously is the simplest and most commonly used strategy for preparing SCCs (**Figure 3**A). The prepared conductive composite has a homogeneous 3D conductive filler network dispersed in the matrix. There are three methods suitable for different types of matrices: direct mixing, solution mixing, and melt mixing. Direct mixing method requires the matrix (such as silicones or fluorinated polymers) to be liquid at room temperature to disperse conductive fillers by stirring.[8d,53,63,64] This method is simple but requires a suitable filler concentration. Fillers with a very small amount are difficult to disperse homogeneously, whereas adding too much filler in the matrix may impede the crosslinking of the elastomer and reduce the mechanical strength of the composite. The solution mixing method is generally used for solid matrices that are difficult to mix directly with fillers. The polymer matrix is dissolved in a volatile organic solvent and mixed with conductive fillers to obtain a homogeneous solution. The organic solvent can be removed by vacuum degassing or heating.[7d,10a,11c,65,66] Another method is to pour the mixed liquid into methanol and precipitate to obtain composites.[10b,67] Compared with direct mixing, composites made by solution mixing generally have better filler dispersion and a wider range of filler content. The melt mixing method is usually used for thermoplastic polymers. The matrices are first melted and blended with the fillers by processing equipment, such as twin screw extruder, and then hot pressed into composites.[51b,68] As this procedure involves high temperature, the conductive fillers are mostly carbon fillers due to their thermal stability.

In the filler-matrix mixing methods, the role of the matrix is to disperse the fillers to obtain a conductive filler network. In contrast, the matrix infiltration method is to immerse the already-formed filler network structure into the liquid polymer (Figure 3B).[7b,11a,13a] Here, the role of the matrix is to fix the filler network to improve stretchability and mechanical strength of the composite. The filler network can be formed by mixing fibrous fillers like CNTs or metal NWs in the solvent before vacuum infiltration.,[7c,8c,69] Another common strategy in the matrix infiltration method is to immerse a conductive sponge or aerogel in the liquid matrix.[70] Conductive sponge has a loose porous structure, generally prepared by freeze-drying method[71,72] or template sponge-based method.[8a,73] In addition, the chemical reduction technique can incorporate conductive fillers into the polymer matrix, such as growing AgNPs in the matrix by reducing silver ions from solution.[8d,74]

2.2.2. Heterogeneous Assembly Method

In homogeneous mixing methods, the conductive fillers in the SCCs are well dispersed in the matrix. In contrast, composites fabricated by heterogeneous assembly methods such as layered assembly techniques have a layered structure composed of a filler

network layer and an elastomer substrate. These methods are commonly used to prepare stretchable conductive films and yarns. Many mature layered assembly methods have been developed, such as surface deposition, drop casting, spin coating, spray coating, and patterning techniques.

Chemical vapor deposition is usually used to deposit graphene on the surface of polymer films or fibers to form a conductive network.[13a,75,76] In addition, it is also a common strategy to deposit metal filler on the surface of the substrate by chemical reduction techniques.[55,77] The common feature of drop casting, spin coating, bar coating, and spray coating is to coat a filler solution on the substrate to form a layered structure, although their specific steps are different (Figure 3C).[1c] The drop-casting method is to dispense the solution of fillers and the volatile organic solvent on the substrate. Capillary action driven by solvent evaporation allows the formation of a tight filler network on the substrate.[56,78] In contrast, the spin-coating and bar-coating methods generally coat a mixture of fillers and liquid polymer matrix to the substrate film and solidify it.[59,79,80] In addition, spin coating is also commonly used to encapsulate layered conductive films.[8b] As the name implies, the spray-coating method sprays the filler solution on the substrate to form a thin conductive coating. This approach can obtain a conductive coating with uniform thickness even on a nonplanar substrate.[9g,81] Recently, a brush-coating method was developed in which the filler solution was directionally coated on the substrate by the brush. This can align the conductive fillers in the substrate to improve the conductivity of the composite film (Figure 3D).[82] Patterning techniques such as screen printing and photolithography can form conductive patterns on thin-film substrates to achieve complex functions (Figure 3E). The screen-printing method deposits conductive ink on the substrate for patterning.[37,83,84d] Although the process is simple, its pattern resolution is low. In contrast, photolithography technique can form high-resolution conductive patterns.[85] In addition, a recently reported AgNP-filled conductive ink achieves direct-write nozzle printing with a minimum feature width of 3 μm to create high-resolution stretchable circuits.[86]

2.2.3. Spinning Method

The spinning method is a special technique for producing stretchable conductive yarns, including wet spinning, dry spinning, electrospinning, and hot drawing (Figure 3F).[87] Traditional wet spinning fabricates long yarns by injecting the mixed solution of conductive fillers and polymer matrix into a coagulating bath such as methanol.[74,88–90] For example, it is possible to form a coaxial structure of conductive yarn of elastomer-wrapped CNT fibers via coaxial wet spinning.[91] Dry-spun yarn is formed by extruding composite solution in hot air.[92] Its production speed is usually faster than wet spinning. Electrospinning technology stretches the polymer solution into silk threads by electrostatic action in an electric field, which can produce multiple yarns simultaneously.[11b,93] In addition, thermoplastic elastomer-based composites can also be directly stretched at a high temperature (depends on the softening temperature of the thermoplastic elastomer) to form yarns.[40a]

2.2.4. Filler Processing Method of Hybrid-Filler Composites

Compared with single-filler SCCs, some hybrid-filler SCCs require additional processing. The main purpose of filler processing is to combine the primary conductive fillers and the secondary fillers. Filler-welding techniques, including hot welding and cold welding, can reduce the contact resistance between adjacent fillers and improve the electrical conductivity of the composite (Figure 3G). Hot welding uses light or Joule heat to fuse the junctions of hybrid metal fillers such as AgNWs and AgNPs to reduce the junction resistance.[35,94] Cold welding sinters nanofiber (NF) fillers through capillary forces generated by solvent evaporation, which is suitable for carbon fillers like CNTs.[11a,95] Incorporating secondary fillers into conductive sponges or fabrics can also significantly enhance the electrical conductivity. Common methods include depositing secondary fillers inside the conductive sponge by dip coating or chemical vapor deposition.[96–98] In addition, recent studies have also introduced the chemical reduction method to chemically plate a metal coating on main fillers to protect or enhance the conductive filler network.[8a,22,99]

3. Stretchability Enhancement Strategies

Achieving both high conductivity and mechanical stretchability simultaneously is a major challenge for SCCs because most SCCs use rigid conductive fillers. Increasing the filler content for achieving high conductivity will also significantly increase the Young's modulus of SCCs and reduce the fracture strain. In addition, under a high tensile strain, the filler networks in SCCs are also easily disconnected, resulting in a sharp decrease in conductivity. Improving the mechanical stretchability of SCCs while maintaining high conductivity is critical for enabling their applications in stretchable electronics. Unless specified specifically, the stretchability mentioned in this Review refers to the mechanical stretchability of the SCCs under the premise of maintaining their electrical conductivity. There are three commonly used strategies for enhancing stretchability, including 1) using intrinsically stretchable fillers, 2) establishing stretchable filler micronetworks, and 3) designing stretchable geometric macrostructures (Figure 1C).[2b]

3.1. Using Intrinsically Stretchable Fillers

Without rigid fillers, SCCs filled with intrinsically stretchable fillers do not suffer from decreased stretchability, resulting from increased filler content. More importantly, the stretchable fillers can also deform along with the elastomer during stretching and therefore, will not disconnect from each other like rigid fillers.[28] Intrinsically stretchable fillers mainly refer to room-temperature LMs.[38a,39b] LMs can maintain constant metallic conductivity under strains limited theoretically only by the mechanical limits of the elastomer.

In one study, polymerized networks of LM microparticles (MPs) comprising >99 wt% LM (by weight) form conductive films when strained.[26a] The polymer shell surrounding the LM particles ruptures when stretched, releasing the LM to form conductive paths. The composite can be elongated by > 700% with nearly constant resistance (**Figure 4**A). In another example, conductive paths

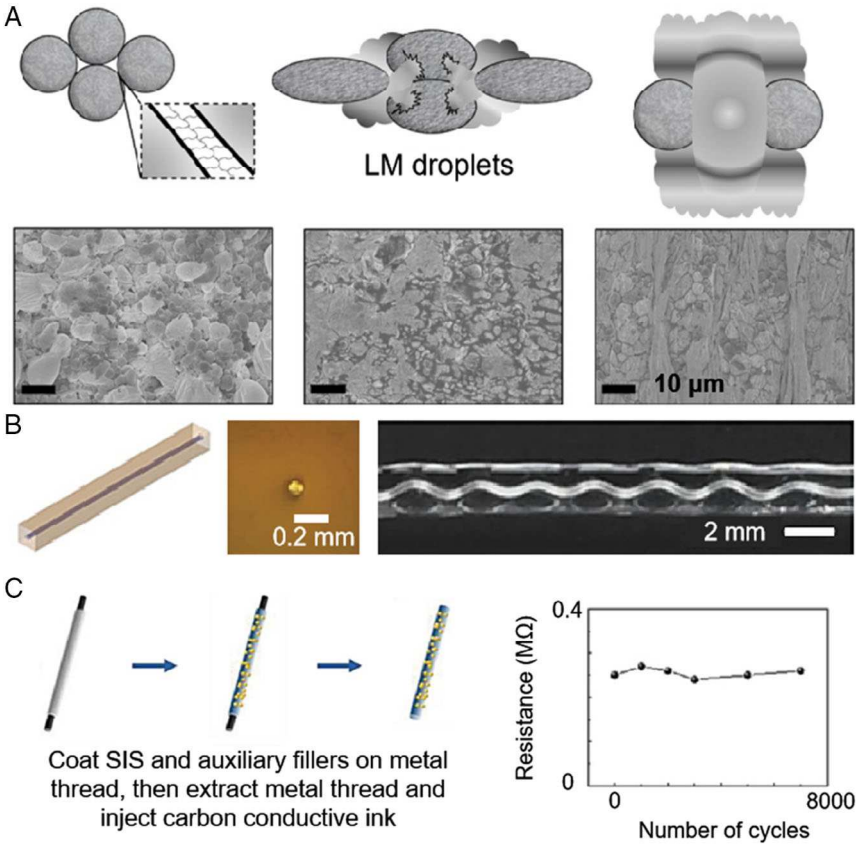

Figure 4. SCCs filled with intrinsically stretchable fillers. A) The process of the rupture of the polymer shell surrounding the LM droplets and releasing the LM to form conductive paths. Adapted with permission.[26a] Copyright 2019, Wiley-VCH. B) The schematic image, cross-section image, and photograph of a polymer yarn injected with LM. Adapted with permission.[40a] Copyright 2018, Wiley-VCH. C) The fabrication method of a conductive ink SIS stretchable wire (left), and its resistance under 8000 stretching cycles. Adapted with permission.[101] Copyright 2019, Wiley-VCH.

between LM droplets are formed by incorporating a small amount of graphene secondary fillers into the PDMS matrix.[7a] In this way, the composite can achieve a high conductivity under deformation without breaking the matrix to release LMs. When used in heterogeneous SCCs, LM can be printed on the polymer substrate[100] or injected into a hollow polymer fiber (Figure 4B).[40a] The mechanical strength and tensile limit of the as-prepared conductive film or yarn depend only on the matrix polymer. Thus, the matrix can be replaced to meet different application requirements.

In addition, conductive composites based on liquid matrices, namely conductive inks, can also be freely deformed like LM. For instance, injecting carbon conductive ink (comprising carbon, graphite, and synthetic oil) into hollow poly(styrene–isoprene–styrene) (SIS) tubes forms highly stretchable wires, although with a much lower conductivity than LM.[101] The conductivity of the wire remained constant even under a 250% tensile strain. In addition, its resistance was almost unaffected over 7000 cycles of consecutive strain cycling tests at 100% strain (Figure 4C).

3.2. Forming Stretchable Filler Micronetworks

3.2.1. Filler Percolation Network

The design of stretchable filler micronetworks can enable the filler network itself to maintain electrical interconnection during stretching. The term "micronetwork" refers here to the shape of the particles and the geometry by which they are connected. Although rigid fillers cannot be elongated themselves, their filler percolation network can rearrange under stretching to preserve the connection of the conductive fillers. Fillers with high aspect ratio like AgNWs,[22,37a,102] CuNWs,[37b,94] or CNTs[37c] can form crisscross fiber percolation networks in the matrix or on the surface of the conductive membrane (Figure 2C). The fiber fillers slide or rotate to align along the elongated direction during stretching, which maintains electrical contact between particles to prevent a rapid increase in resistivity. Compared with fibrous fillers, NPs may not appear to be candidates for enhancing the stretchability of composites. Their percolation threshold is 10–100 times higher than that of nanofillers with high aspect ratios, and NPs with strong attraction to polymers can cause the matrix to harden. However, NPs in the matrix can move more freely than that of NFs that are restricted by shape; this is critical for the stretchability of NP-filled composites. As the electrical connection between NPs does not depend on their mutual orientation, the conductive paths destroyed during deformation can be recovered by the movement and reconnection of NPs, which is difficult for nanotubes or NWs to achieve.[62b] For example, AuNPs filled in a polyurethane conductive film can aggregate and assemble into chains of particles along the elongation direction, thereby slowing down the decrease in conductivity during

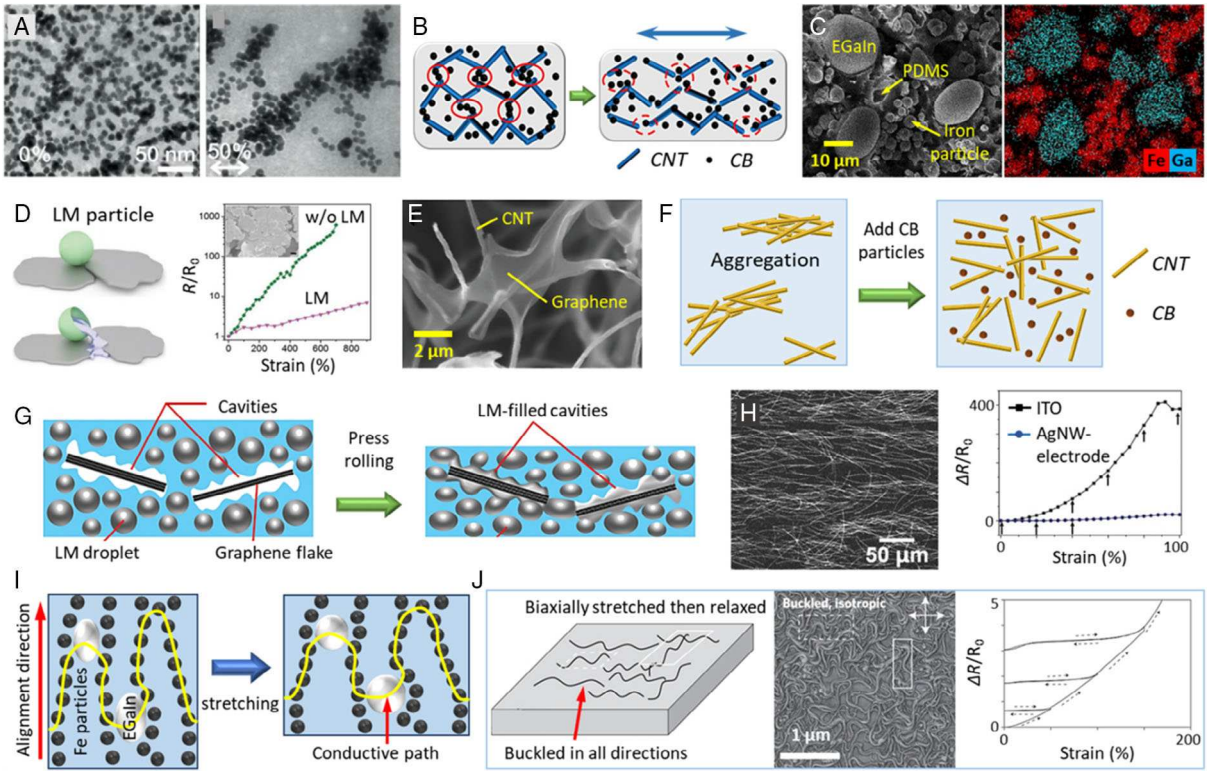

Figure 5. SCCs using the stretchable filler micronetwork designs. A) As the strain increased, the AuNPs in the polyurethane conductive ultrathin film gradually reorganized into bands along the stretching direction. Adapted with permission.[62b] Copyright 2013, Springer Nature. B) The schematic illustration of the change of CNT–CB filler networks during stretching. Adapted with permission.[7d] Copyright 2018, Elsevier. C) SEM images and energy-dispersive X-ray spectroscopy (EDS) element mappings of the LMMRE. Adapted under the terms of the CC-BY 4.0 license.[103] Copyright 2019, The Authors, published by Springer Nature. D) The LM particles rupture to bridge silver flakes when stretched (left). The comparison of the relative resistance–strain curves of SCCs filled with/without LM (right). Adapted with permission.[36] Copyright 2018, Wiley-VCH. E) SEM image of CNT junctions welded with graphene. Adapted with permission.[7b] Copyright 2019, Wiley-VCH. F) The schematic images of using CB secondary fillers to disperse CNT aggregates and form a uniform percolation network. G) Schematic diagram of pressing LM into the cavities between graphene flakes and the matrix using press-rolling procedure to promote the interconnection of the main and secondary fillers. Adapted with permission.[7a] Copyright 2019, Wiley-VCH. H) SEM image of the anisotropic AgNW electrode (left) and the comparison between its relative resistance change–strain curve along alignment direction and that of an indium tin oxide electrode (right). Adapted with permission.[107] Copyright 2018, Wiley-VCH. I) The change of microstructure and conductive path of the anisotropic composite filled with Fe–EGaIn hybrid fillers when stretched perpendicular to the alignment direction. Adapted with permission.[109a] Copyright 2020, Elsevier. J) The schematic image, SEM image, and relative resistance change–strain curve of a CNT–PDMS composite with random spring-like CNT networks. Adapted with permission.[76b] Copyright 2011, Springer Nature.

stretching (**Figure 5**A).[62b] The conductivity of this composite film only dropped by four times under a tensile strain of 110%.

Many recent studies on hybrid-filler SCCs used auxiliary fillers to enhance the percolation network. One strategy is to fill the secondary fillers in the gap of primary fillers to form a dense percolation network.[7a,c] When the composite is elongated, these secondary fillers can still bridge the primary fillers to maintain high conductivity. For instance, the CNTs filled in a highly stretchable PDMS-based composite can be bridged by conductive CB particles to enhance the density of the filler network, increasing the composite's conductivity by two orders of magnitude (Figure 5B).[7d] At 300% strain, the resistance of the composite only increased by 13 times, showing a superior tensile limit and stability in conductivity under tension to most SCCs. In another case, researchers sprayed AgNWs on a silver NF (AgNF) network to obtain a conductive film with a sheet resistance as low as $1\,\Omega\,sq^{-1}$.[7e] These AgNWs can bridge across the locally disconnected areas of the NF network to preserve the low resistance. The sheet resistance of the film was only increased by 28% at a 90% tensile strain. Moreover, LM is also an ideal choice as the bridge filler due to its excellent deformability.[21,41] For instance, an LM-filled magnetorheological elastomer (LMMRE) comprising a hybrid of fillers of EGaIn droplets and iron MPs has interesting properties.[103] The diameter of EGaIn droplets is about ten times that of iron particles, so it can bridge a large number of conductive particles. The scanning electron microscope (SEM) image of the LMMRE sample and the distribution diagram of LM droplets and iron MPs intuitively reflect the conductive percolation network formed by them (Figure 5C). When the composite is deformed, the EGaIn droplet deforms along with the matrix and keeps contact with the surrounding iron particles, which ensure the high conductivity of the composite under any mechanical deformation. In contrast, composites only filled with iron powder (without LM) are insulators under any mechanical loadings. Likewise, it is possible to prepare a SCC with a fracture strain of up to 1000% using silver flakes and EGaIn fillers.[36]

During stretching, EGaIn droplets filled the gaps between the silver sheets to repair the conductive network. The resistance of the composite using only silver flakes increased dramatically by 600 times at a strain of 700%. As a comparison, the resistance of the composite using EGaIn only increased by 3.7 times at the same strain (Figure 5D). In summary, the secondary fillers used to bridge the primary fillers are usually particulate fillers or metal NWs with smaller sizes than primary fillers or LMs with high deformability and fluidity.

Another method to enhance the percolation network is to weld the primary fillers with secondary fillers to reduce the junction resistance. For example, graphene can weld loosely contacted CNTs to enhance the electron transfer across the CNT junctions.[7b] Graphene welding at the junction can provide high structural stability and electrical conductivity under tension by hindering the interfacial slippage of CNTs (Figure 5E). Similarly, depositing soft AuNWs on a network of AgNWs enhances the stretchability of the conductive composite film.[56] AuNWs act as flexible conductive bridges to strengthen the connection points between AgNWs. As the deposition amount of AuNWs increases, the sheet resistance of the conductive film decreases significantly under a high tensile strain, reflecting the improvement in conductivity and stretchability.

As mentioned earlier, most carbon fillers tend to aggregate, which is not conducive to the formation of uniform percolation networks. To solve this problem, many recent studies have used auxiliary fillers to promote the homogeneous dispersion of carbon fillers in the matrix.[3b–d,5] The synergistic effect of the primary filler and the secondary filler forms a uniform percolated network, which increases both the electrical conductivity and the stretchability of the SCCs (Figure 5F). For instance, calcium hydroxide nanospherulites help to disperse graphene sheets homogeneously in a polyacrylamide hydrogel matrix.[5a] The obtained conductive hydrogel exhibited excellent conductivity and long-term stability upon elongation. After five times elongation, its resistance was only 3.3 times that of the relaxed state. Likewise, in a CP composite composed of Ecoflex matrix and hybrid fillers of CNTs and CB, the CB particles avoid 1) the aggregation of CNTs during the preparation process and 2) the separation between CNTs when stretching the composite.[65] As a result, the composite was found to increase only 40% in resistance at a 200% strain.

Some postprocessing procedures, such as press rolling or hot rolling, can also promote the percolation of conductive fillers or increase the stretchability of SCCs. The conductivity of stretchable conductors containing EGaIn droplets and graphene sheets can be enhanced via a press-rolling procedure.[7a] Press rolling promotes the interconnection of the EGaIn droplets with secondary fillers and also their percolation in the PDMS matrix (Figure 5G). This procedure significantly improved the conductivity of the composite by eight orders of magnitude. Furthermore, the mechanical stretchability of a Ag−Au nanocomposite increases from 266% to 840% through the heat rolling-press process.[22] Likewise, this hot rolling can produce highly conductive and stretchable hybrid composites composed of silver microflakes, multiwalled carbon nanotubes (MWCNTs), and poly(vinylidene fluoride) (PVDF) copolymer.[104] After the hot rolling process, its mechanical stretchability and initial conductivity were improved by 342% and 190%, respectively.

3.2.2. Alignment of Fillers

For conductive composites that only withstand uniaxial strain, prealigning the conductive fillers along the elongation direction can significantly improve conductivity and stretchability. When stretched, the conductive fiber fillers will slide along the tensile direction and maintain electrical connection with each other, resulting in better alignment without damaging the conductive network. The disadvantage of this strategy is that it is only effective for uniaxial stretching and not suitable for biaxial stretching. Recently, a variety of techniques have been developed to align fiber fillers on substrates, such as dip coating,[105] grazing-incidence spraying,[106] directional brush coating,[107] and agitation-assisted assembly approach.[108] Brushing a AgNW solution on a poly(ethylene terephthalate) (PET) substrate can obtain an anisotropic transparent electrode, whose conductivity along the brushing direction is over 270 times that of the spin-coated electrode.[107] During stretching, AgNWs slid along the alignment direction to preserve electrical contacts. Under large deformation, the growth in resistance was two orders of magnitude lower than that of the commercial indium tin oxide electrode (Figure 5H). However, many anisotropic SCCs exhibit higher strain sensitivity in the alignment direction. In the direction perpendicular to the alignment, the resistivity of these composites is higher but more stable under strain.[109] Based on these composites, researchers have developed strain sensors that can recognize the direction of strain.[109b,110]

In addition, poststrain treatment can also align the fiber fillers along the stretching direction. Poststrain refers to a stretching step after forming the composite. For example, roughly aligned MWCNTs filled in a PU matrix can be further aligned by stretching and relaxing the composite ten times at 100 °C.[111] This procedure produced a stable aligned filler network in the matrix, ensuring the composite to have a substantially constant conductivity at 30% strain (100% poststrain). Similarly, a stretchable conductor film consisting of well-aligned CNT ribbons embedded in a film of PDMS becomes more stable with poststrain.[112] When the film was stretched for the first time, its resistance increased by 1.5 times at a 120% strain and partially recovered after being released back to the relaxed state. In the subsequent stretching cycles, the film resistance remained stable in the range of 0–100% tensile strain, indicating that poststrain enhanced the stability of conductivity under stretching.

In addition to aligning fiber fillers along the stretching direction, the conductivity and stretchability of an anisotropic SCC filled with Fe MPs and EGaIn microdroplets can be improved by magnetically aligning the Fe particles prior to curing the elastomer. Interestingly, the alignment direction of the iron particles was not along but perpendicular to the stretching direction, which was different from all SCCs that improved conductivity by aligning fiber fillers along the stretching direction. In the direction perpendicular to the alignment, Fe particle chains and EGaIn droplets formed a serpentine-shaped conductive path (Figure 5I). Compared with isotropic composites with randomly distributed Fe particles, serpentine-shaped conductive paths increased the conductivity of anisotropic composites by two orders of magnitude. Furthermore, when stretched perpendicular to the alignment direction, the

composite was compressed in the alignment direction, so the distance between the iron particles in the conductive path was reduced, which greatly reduced the electrical resistance (Figure 5I). Its electrical conductivity increased by 52 times at a tensile strain of 20%.

3.2.3. Buckled Fiber Fillers

For SCCs using fibrous conductive fillers, the formation of buckled fiber fillers in the matrix through prestrain or poststrain treatment is also a strategy to improve the stretchability of the composite.[25b] For the case of prestrain, the fiber fillers are deposited on the prestretched substrate, after which the prestrained substrate is released to generate wavy conductive fibers in the matrix. During stretching, the buckled fiber fillers gradually return to the straight state, and the sheet resistance of the composite can remain basically stable. After reaching the prestretched strain, the fillers are completely straightened, and the filler networks begin to break. Therefore, most composites can only maintain a constant resistance below the historical prestretched strain. A previous study embedded CNT ribbons in a 100% prestretched PDMS substrate to fabricate highly stretchable conductors.[113] When the conductor was stretched by 100% to the prestretched strain, its resistance only increased by 4.1%. However, continuing to stretch the composite beyond this strain resulted in a significant increase in resistance. In addition, prestrain can also produce the deformed fiber filler networks. Researchers deposited crossed-aligned AgNW networks on a 50% prestretched PDMS film using layer-by-layer agitation-assisted alignment.[108] The orthogonal networks deform into a tangled and oriented structure in the released state, resulting in an increase in the junction resistance between AgNWs. When the composite was stretched, AgNWs changed from the tangled orientation to the oriented mesh nanostructures, in which the junction resistance decreased and thus the electrical conductivity was improved. The sheet resistance of the conductive film decreased by 80% at a tensile strain of 40%, exhibiting unique negative piezoresistivity.

For the case of poststrain, the prepared conductive composite filled with fiber fillers is repeatedly stretched and released. The fiber fillers slide in the matrix upon stretching and buckles upon releasing. Apart from this, its mechanism of enhancing the conductivity and stretchability is the same as that of prestrain. Composites undergoing poststrain also exhibit a dependence on strain history, which means that their resistance is basically constant at low strains and increases rapidly after exceeding historical poststretched strain.[114] As an example, a PDMS-based SCC incorporating CNTs formed buckled CNTs by repeatedly stretching and releasing the composite.[115] When stretched, the resistance of the composite was constant initially and increased linearly after the poststretched strain. In addition, this method can also be used to improve the stretchability of biaxially stretched SCCs. By applying poststrain to a PDMS film deposited with randomly distributed CNT networks, random spring-like CNT structures can be generated on the substrate.[76b] Under the historical maximum strain along each direction, the composite film can maintain a relatively stable and high electrical conductivity (Figure 5J).

3.3. Designing Stretchable Geometric Macrostructure

By designing stretchable geometric structures, SCC samples can elongate with minimal strain of the filler networks. This approach not only maintains the high conductivity of the sample during stretching but also increases its fracture strain to improve the stretchability.[1d,2b]

3.3.1. Wavy Surface Structure

Through the prestrain and poststrain techniques mentioned in Section 2.2, a wavy fold surface can be formed on a SCC film. Upon stretching, the wavy structure gradually stretches to accommodate the strain, resulting in a much less strain inside the percolation network and thus a nearly constant resistance of the composite (**Figure 6**A). This strategy has been widely used in the fabrication of stretchable conductor films in recent years.[95,116] A recent study prepared an ultrastretchable hybrid-filler electrode composed of AgNWs and MWCNTs through prestretching.[95] The wrinkled surface resulted in an increase in resistance as low as 42% at a uniaxial strain of 580%. Unlike other prestrained composite films that can only keep stable resistance under uniaxial stretching, this hybrid electrode can withstand biaxial stretching and show an increase in resistance of only 100% at a 200% equibiaxial strain. Another study formed a layer of AgNW−PDMS conductive film on the surface of PDMS substrate by the matrix infiltration method and then repeatedly stretched it to 80% strain to produce a wavy structure.[116d] However, its resistance was constant only below a 50% strain, not 80% of the poststrain.

The stretchability of SCC fibers can also be improved by similar methods. Plating a layer of gold film on the surface of a 600% prestrained AuNW−poly(styrene-ethylene-butylene-styrene) (SEBS) composite fiber can obtain a highly stretchable conductive fiber.[92] This process formed a wrinkled gold film on the fiber surface. During stretching, the flatted wrinkles maintain the conductive paths, resulting in an increased conductivity under tensile strain (Figure 6B). Similarly, another study reported highly stretchable conductive fibers fabricated by wrapping CNT sheets oriented along the fiber direction on 1400% prestretched SEBS fiber cores.[76a] The resulting periodic hierarchical buckling structure enabled an increase in resistance of only 4.5% when the fiber was stretched by 1000%.

3.3.2. Serpentine and Spiral Structures

Processing conductive composites into serpentine samples[8c] or patterning conductive fillers on elastic substrates into serpentine circuits[85,117a] can effectively improve their stretchability. However, most of these composites cannot preserve a constant resistance during stretching. This is because the stress will be concentrated in peaks and valleys of the serpentine trace upon stretching, resulting in a higher local tensile strain. For instance, a conductive composite consisting of a Cu−Ag core−shell NW felt is patterned to create serpentine circuits that can power the light-emitting diodes (LEDs) under a strain of up to 300%.[8c] At a 225% tensile strain, the serpentine circuit was completely straightened, with a tenfold increase in resistance (Figure 6C).

In addition, the conductive composite can also be processed into a spiral structure to obtain exceptional stretchability.

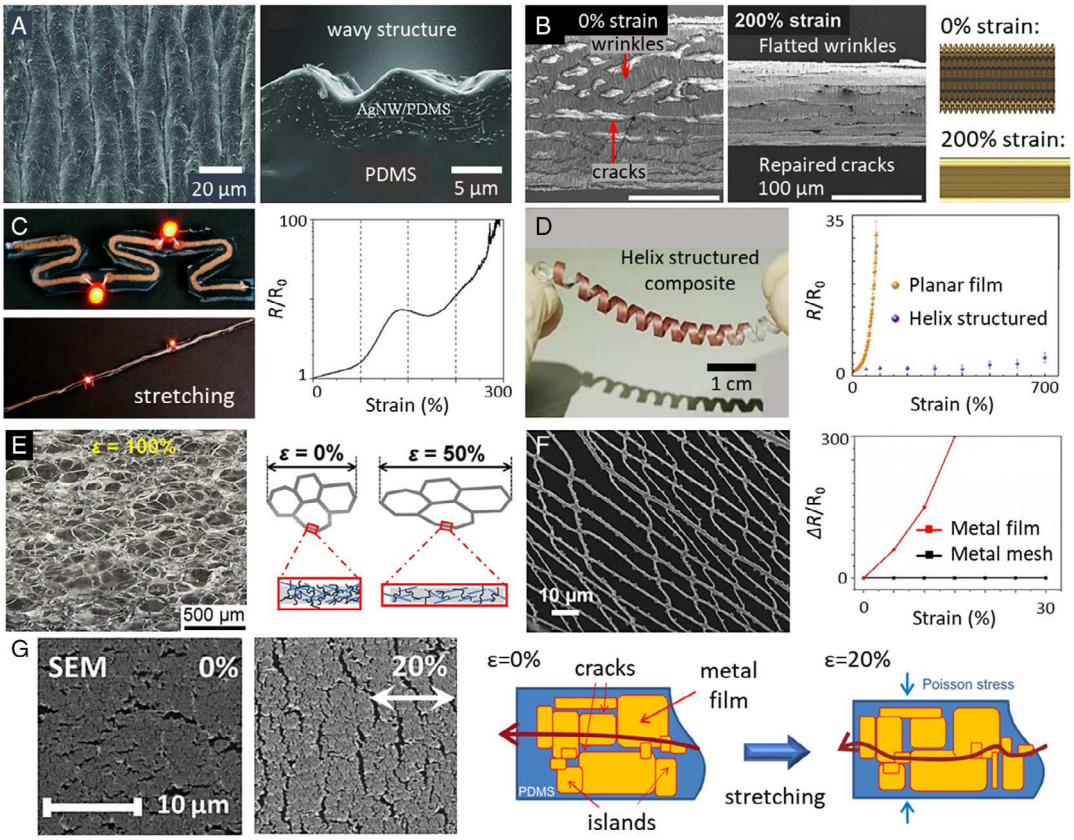

Figure 6. SCCs with stretchable geometric macrostructures. A) The SEM images of the surface and cross section of the AgNW−PDMS electrode with a wavy surface structure. Adapted with permission.[116d] Copyright 2012, Wiley-VCH. B) The SEM images and schematic images of the AuNW–SEBS composite fiber with a wrinkled surface structure under 0% and 200% tensile strain. Adapted with permission.[92] Copyright 2018, Wiley-VCH. C) The photograph of a serpentine LED circuit under 0% and 300% tensile strain (left) and the relative resistance–strain curve of the serpentine circuit (right). The serpentine circuit is made of a Cu–Ag core–shell NW felt infiltrated with the silicon elastomer. Adapted with permission.[8c] Copyright 2018, American Chemical Society. D) The photograph of a helix-structured CuNW–PDMS conductor (left) and its relative resistance–strain curve compared with the planar composite film. Adapted with permission.[116b] Copyright 2014, Springer Nature. E) The optical microscope image of a porous structure composite immersed with PDMS under 100% stretching (left) and its schematic images under stretching. Reproduced with permission.[96] Copyright 2019, Wiley-VCH. F) The SEM image of a composite membrane with a mesh fiber filler structure (left) and its relative resistance change–strain curve compared with the metal film. Adapted with permission.[120] Copyright 2017, American Chemical Society. G) The SEM images and schematic images of a PDMS membrane with gold surface film under 0% and 20% tensile strain. Adapted with permission.[121b] Copyright 2009, AIP Publishing.

Upon stretching, the uniform stress distribution in a 3D spiral structure can suppress local strain. Therefore, its fracture strain is generally higher than that of the 2D serpentine structure.[2a] One representative study presented a helix-structured CuNW−PDMS conductor, which exhibited unprecedented mechanical stretchability of 700% with a resistance increase of only 3.9 times.[116b] As a comparison, the resistance of the CuNW−PDMS conductor film of the same composition increased by 30 times at 100% elongation (Figure 6D). However, serpentine and spiral structures exhibit disadvantages in the larger footprint and longer pathway relative to interconnects forming straight lines.

3.3.3. Porous and Fabric Structures

Conductive composites with porous or fabric structures also exhibit high stretchability. Conductive sponges are the most common porous-structured SCCs, usually prepared based on commercially available nickel[97] or polyurethane[96] foam templates or by sublimating frozen solvents through the freeze-drying technique.[70] However, similar to the serpentine structure, a hollow conductive sponge is prone to form local stress concentration and tear when stretched. To solve this problem, the aforementioned matrix infiltration method is generally used to protect the filler network to enhance the mechanical stretchability and conductivity of the conductive sponge under strain (Figure 6E). Self-healing and superstretchable aerogel conductive sponges can be prepared by unidirectional freezing and matrix infiltration techniques.[118] The composite exhibited a high conductivity of 93 S cm^{-1} and excellent electromechanical stability up to 800% tensile strain. When stretched by 500%, its resistance only increased by 130%. In addition to the traditional conductive sponges, another study produced an interesting bionic porous conductive composite with buckled/collapsed cells through the

fermentation of yeast during the gelling process of the silicone matrix.[16a] Compared with the composite based on unfermented homogeneous elastomer, its tensile limit increased by ≈80%. During stretching, the electrical resistance of this composite unconventionally decreased, showing negative piezoresistivity.

The conductive composites with a fabric structure can reduce the microscopic strain of the percolation network through the dislocation and structural deformation of the fabric fibers. In one example, a wrinkled fabric was dipped into an MWCNT−PDMS dispersion to fabricate stretchable and flexible electronic skins with a relatively stable resistance.[48c] Instead of using fabric templates, another approach reported a highly stretchable conductive fiber mat composed of AgNP−poly(styrene-butadiene-styrene) (SBS) composite fibers.[119] The tensile limit of a single composite fiber was only 60%. The fiber mat, however, can be stretched up to 140% with a high conductivity of 600 S cm^{-1}. In addition, the mesh fiber filler structure allows the composite membrane to have high mechanical stretchability and stable electrical conductivity. Silver submicron fibers can also be woven into a mesh structure and transferred onto a PET substrate to prepare a stretchable transparent electrode.[120] The electrode can withstand 30% elongation with a resistance change within 12% (Figure 6F).

3.3.4. Other Geometric Structures

Apart from the aforementioned strategies, other geometrical structures have also been developed to improve the stretchability of elastic conductors, such as microcracking, perforation, topology structure, and planar meandering structures.

For an elastic substrate coated with a metal film, common methods to improve mechanical stretchability usually seek to avoid the generation of microcracks on the metal film as cracks can damage the conductor. However, the regular formation of cracks on a metal film can unexpectedly enhance the mechanical stretchability of the conductive film.[27,121] Under tensile strain, these cracks can relieve most of the strain to protect the metal film from electrical disconnection. For example, a 50 nm-thick gold thin film on a PDMS membrane forms an interconnected mud-like crack pattern.[121b] Its resistance remained finite and reproducible over 250 000 cycles of 20% stretching (Figure 6G).

In addition, it is also possible to increase the mechanical stretchability of the SCC film by punching round holes.[104] The perforation can lead to discontinuous stress distribution and increase the elasticity of the composite during stretching. By introducing two circular holes with a diameter of 1 mm into the Ag-MWCNT conductor film, the tensile limit of the Ag-MWCNT film embedded in the nitrile rubber substrate increased from 75% to 120%. Finally, screen-printed kirigami topology structures[122] and wet-etched metal microwire planar meandering structures based on complex interconnect designs[123] can also provide excellent stretchability for conductive composites.

4. Numerical Simulation and Theoretical Analysis

Various models and theories exist to simulate and analyze the electrical properties of SCCs in the relaxed state or under mechanical deformation. This section will briefly introduce the static analysis methods for the electrical properties of SCCs and then analyze their strain responses in detail.

4.1. Static Analysis

4.1.1. Common Numerical Models

Since the advent of conductive composites, there have been numerous studies to calculate their electrical conductivity through numerical simulations, attempting to obtain a model that can fit the experimental results. A variety of numerical models have been developed around this purpose, and the percolation model is the most widely used among them. The percolation theory is used to describe the relationship between the conductivity of the conductive composite and the filler concentration. It assumes that when the filler volume fraction exceeds a certain critical value (called the percolation threshold), a connected filler network will be formed across the composite, causing the system to percolate and conduct electricity. At the critical volume fraction, the conductivity of the composite suddenly increases by several orders of magnitude and transforms from an insulator to a conductor, which indicates the existence of the percolation threshold (**Figure 7**A).

According to the percolation theory, the conductivity of the composite composed of conductive particle fillers and insulating matrix satisfies the following equation.[124]

$$\sigma = \sigma_0 (f - f_p)^t \quad (1)$$

where σ is the conductivity of the composite, σ_o is a scaling factor proportional to the conductivity of the filler, f and f_p are the volume fraction and percolation threshold of the conductive filler, respectively, and t is the critical exponent. This simple power law equation is valid when the filler volume fraction is above the percolation threshold ($f > f_p$). As the most important parameter in percolation theory, the percolation threshold is mainly determined by the size and shape of the conductive filler. Fillers with small sizes and high aspect ratios commonly have low percolation thresholds. Researchers predicted and formulated the percolation thresholds of spherical, plate, and nanotube fillers in polymer composites through simple and effective cubic unit cell models. These formulae verified the relationship between the percolation threshold and the size and aspect ratio of fillers (Figure 7).[125]

The critical exponent t is related to the geometry of the filler and the dimensions of the composite. The theoretical values of t in 2D and 3D model systems are commonly about 1.3 and 2.0, respectively.[126] It generally increases with the increase in aspect ratio of the filler, which means that the critical exponent of the fiber filler is usually higher than that of the spherical filler. However, a wide range of t values from 1 to 10 has been reported, especially for 1D fiber fillers.[127] For example, a previous study reported a microfibrillar anisotropic composite with a selective CB distribution on the surfaces of the PET microfibrils.[128] Due to the complex anisotropic distribution of CB particles, its critical exponent t was as high as 6.4, which greatly deviated from the universal percolation theory.

In addition to the most popular percolation theory, other models have also been proposed in recent decades, including

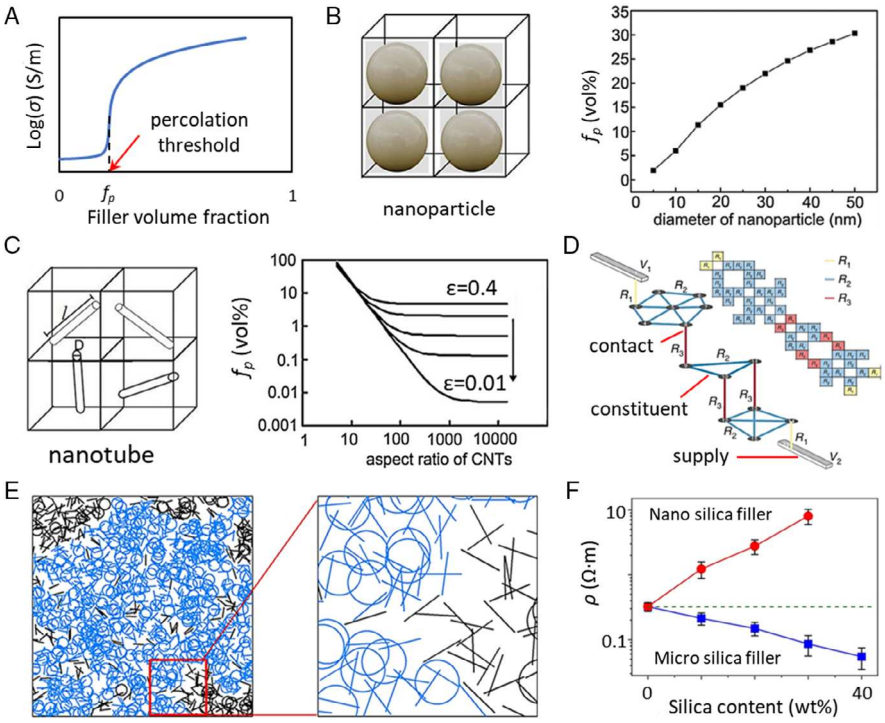

Figure 7. Static analysis of the electrical properties of SCCs. A) The conductivity—filler volume fraction curve reflects the existence of percolation threshold. B) The 3D random distribution model and percolation threshold—particle diameter curve of NPs. Adapted with permission.[125b] Copyright 2007, Elsevier. C) The 3D random distribution model and percolation threshold—aspect ratio curve of nanotubes. ε is the dispersion parameter, low ε represents a small aggregation of CNTs. Adapted with permission.[125a] Copyright 2007, Wiley-VCH. D) Schematic illustration of connections within and between nanostructures (materials, junction, and contact resistances are denoted by R_1, R_2, and R_3, respectively, resulting in a voltage difference (V_1-V_2) between the electrodes). Inset shows the corresponding resistance adjacency matrix. Adapted with permission.[130] Copyright 2020, Springer Nature. E) Graphic representations of a continuum of a 2D disk–stick percolation model. Reproduced with permission.[131] Copyright 2018, IOP Publishing. F) Resistivity of the CNT/silica composites under different silica contents and sizes for fixed CNT contents (1 wt%). Adapted under the terms of the CC-BY 4.0 license.[133] Copyright 2019, The Authors, published by Springer Nature.

tunneling model, effective media model, thermodynamic model, Bueche model, Nielsen model, McCullough model, Ondracek model, and Cahn-Hilliard model.[126,129] These models have their own scope of application and are superior to percolation models under certain conditions. Strictly speaking, the percolation theory is only applicable when the matrix is completely insulating, which is problematic in many practical systems. Furthermore, the percolation model is only valid when the filler volume fraction is far below the maximum fillable concentration and above the percolation threshold. Therefore, it is impossible to make an accurate estimate of the conductivity at a wide range of filler concentrations. By comparing simulation and experimental results, one study proved that for graphene-filled polymer blend nanocomposites, the conductivity predicted by Mamunya's thermodynamic model was closer to the experimental results than that of the percolation model. The Mamunya model takes into account the filler and polymer surface energies as well as the polymer–filler interactions and thus accurately predicts the electrical conductivity of the composite under high filler content.[129b] Different from percolation theory, Bruggeman's effective media theory comprehensively considers the electrical conductivity of the filler and matrix. The general effective media equation, which combines most aspects of both theories, describes the conductivity of filler/matrix binary composites. The proposed piecewise equation covers all filler volume fractions from 0% to 100%, which greatly improve the percolation theory.[129c] When simulating the electrical properties of composites, it is necessary to select appropriate numerical models for different filler/matrix compositions and verify with experimental results.

4.1.2. Simulation of Hybrid-Filler Composites

It is difficult to simulate the conductivity of hybrid-filler composites. Different conductive fillers have different shapes and sizes, so the hybrid fillers have extremely complex spatial distribution in the matrix. This invalidates the classic percolation model, because the percolation conductivity equation is only applicable to an ideal system containing well-dispersed fillers of the same shape and size. As a result, it is almost impossible to derive the conductivity equation of the hybrid-filler composite. There are only a few equations that are valid for specific filler shapes, proportions, and distribution methods and therefore cannot be generalized to other composites.

Many recent studies abandoned the derivation of the conductivity formula of hybrid-filler composites and turned to establish the filler network model by the Monte Carlo method and

simulate the conductivity of composites based on percolation theory. Monte Carlo simulation, also known as statistical experiment simulation, refers to the random generation of filler networks in a 2D or 3D model by the computer and then calculating its electrical conductivity by finite element software. Its advantage lies in relying mainly on software calculation, eliminating a large amount of mathematical derivation processes. In theory, as long as the filler network model and condition settings are consistent with real composites, the simulation result will be close to the experimental data. To conduct quantitative analysis and reduce the deviation of the simulation results from the experiment, it is also necessary to optimize the filler model and modeling method according to the specific situation and set appropriate simulation parameters. For example, a recent study introduced a universal discretization approach to convert the 3D nanostructure of conductive composites into complex resistor network graphs (Figure 7D). Using a simple solver tool, the resistance of the resistor network can be calculated by solving Kirchhoff's law. For various filler shapes and concentrations, simulation results based on this improved modeling method showed good agreement with the experimental data.[130] Although accurate conductivity formulae cannot be derived through Monte Carlo simulation, it can still be used to quantitatively analyze the relationship between filler geometric properties or concentration and the conductivity of the composite.

Real and effective modeling is the first and most important step in Monte Carlo simulation. A 2D disk–stick percolation model for Monte Carlo simulation was developed to describe the percolation behavior in composite membranes containing 1D and 2D conductive nanofillers.[131] This model successfully predicted the electrical percolation thresholds of the conductive composite membranes, which have also been qualitatively validated by experimental results (Figure 7E). Optimizing the aggregation degree of CB and the 3D model of CNTs greatly narrowed the deviation between the results of simulation and experiment.[132] This indicated that it is feasible to quantitatively analyze the electrical percolation of the hybrid-filler composites filled with CB and CNTs by Monte Carlo simulation. The Monte Carlo method can also analyze the effect of secondary particulate fillers on the conductivity of composites through the combination of Voronoi geometry and percolation theory.[133] Such simulation results showed that the conductivity of the composites filled with CNTs and secondary spherical silica fillers depends on the size of the silica filler. Micrometer-scale silica fillers could increase the density of CNT networks and the conductivity. However, the nanoscale silica fillers would destroy the CNT percolation networks and therefore reduce the electrical conductivity (Figure 7F). Furthermore, Monte Carlo simulation can also calculate the electrical percolation threshold of CB-CNT hybrid-filler composites.[5b] The simulated percolation threshold decreased with the increase in CNTs' aspect ratios and decrease in the diameter of CB aggregate, which was consistent with the percolation theory. In addition, earlier studies also confirmed the synergistic conductive effect of the main and secondary fillers in hybrid-filler composites. This effect promotes the dispersion of aggregated fillers and reduces their percolation threshold, which improves the electrical conductivity of composites.

4.2. Strain Response Analysis

In addition to analyzing the static conductivity of SCCs, it is also important to study the change of their electrical conductivity under mechanical deformations such as stretching, compression, and bending. In this section, we will first introduce general theories on the strain response of the electrical conductivity of SCCs. Subsequent sections will detail the four piezoresistive characteristics of SCCs, namely, positive piezoresistivity, negative piezoresistivity, strain insensitivity, and special piezoresistivity.

4.2.1. General Theories of Strain Response

When a conductive composite is deformed, the destruction and formation of the filler conductive networks can occur simultaneously. The change in electrical conductivity is a result of both phenomena, and the dominant phenomenon determines the piezoresistive property of the composite.[46a] For instance, under uniaxial pressure, there are three possible changes in the conductive paths in the spherical particle-filled composite.[134] The first is the increase in existing conductive paths. Uniaxial compressive pressure results in a reduction in the gap between the particle fillers, thereby reducing the resistance of the existing conductive paths (**Figure 8**A). The second is the destruction of existing conductive paths. The particulate fillers in close contact are squeezed out from the existing conductive path under compression, causing the conductive path to fail (Figure 8B). The third is the formation of new conductive paths. Uniaxial compression reduces the distance between dispersed fillers, thereby forming new conductive paths (Figure 8C). These three changes work concurrently and jointly determine the piezoresistive properties of the conductive composite.

In addition, the Poisson's ratio of composites is also a key parameter that affects the change of conductivity during deformation.[104] The Poisson's ratio determines the change in the total volume of the composite and the electrical contact concentration of the conductive fillers. Take the spherical particle-filled composite as an example. If its Poisson's ratio is very small, during compression, the volume of the sample will decrease, and the filler concentration will increase. This causes a significant decrease in the average distance between fillers and an increase in the electrical contact concentration. As a result, the electrical resistivity of the composite decreases, exhibiting a positive piezoresistivity. Conversely, when the Poisson's ratio is very close to 0.5, it can be approximated that the volume of the composite is constant during deformation. Therefore, the concentration as well as the electrical contact concentration of spherical particles in the matrix will not change during deformation, making the conductivity insensitive to strain. When filled with irregular fillers, the electrical contact concentration in the composite may even increase during stretching, exhibiting negative piezoresistivity.[103]

Under mechanical deformation, the conductivity of SCCs changes with strain. The rate of change, i.e., the strain sensitivity of the conductivity, depends on the concentration, type and geometric characteristics of the fillers, the mechanical properties of the elastic matrix, and the manufacturing process of the

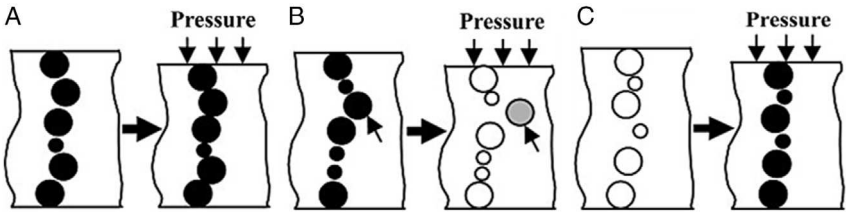

Figure 8. Three changes in conductive paths in the composite under uniaxial pressure: A) the enhancement of existing conductive paths, B) the destruction of existing conductive paths, and C) the formation of new conductive paths. A–C) Adapted with permission.[134] Copyright 2007, Wiley Periodicals, Inc.

composites.[46a] Generally, when the filler content is very high, a percolation network with high concentration will be formed in the composite to maintain a relatively stable electrical conductivity during deformation, thus exhibiting lower strain sensitivity. In addition, composites filled with rigid fillers are also more sensitive than composites filled with liquid fillers. For composites with randomly and homogeneously dispersed fillers, as stated in Section 1.1, the higher the aspect ratio of the fillers, the lower the strain sensitivity of the composites. Manufacturing processes also affect strain sensitivity. One study demonstrated that aligning CNTs in the matrix can increase the strain sensitivity of the composite.[135] Likewise, another study achieved the same effect by reducing the curing temperature and increasing the mixing rate during the preparation process.[136] Furthermore, some recent studies have also enhanced[35,79] or weakened[21,31,36,65] the strain sensitivity of SCCs by adding secondary fillers. These hybrid-filler systems can simultaneously improve the stretchability and adjust the strain sensitivity of composites, which are superior to single-filler systems.

4.2.2. Positive Piezoresistivity

The vast majority of conductive composites exhibit a positive piezoresistive effect, that is, their resistivity decreases when compressed and increases when stretched. This is in line with intuition: compression causes the conductive fillers to come closer to each other, and electrons are more likely to transfer between the fillers and thus the resistivity decreases. In contrast, under stretching, the conductive paths are disconnected and the resistance increases.

The change in the resistivity of composites under strain is usually not linear. The resistance of SCCs with positive piezoresistivity generally decreases rapidly at the beginning of compression and tends to stabilize with further compression. This is because when compression starts, the fillers are close to each other, forming a large number of conductive paths. As the compressive strain increases, the generation rate of conductive paths reduces and the downward trend of resistance slows down. Eventually, the number of conductive paths tends to saturate and the resistance is basically stable. As proof, one study reported a PDMS-based high-sensitivity pressure sensor filled with CNTs and graphene.[137] When the surface pressure was lower than 0.3 kPa, the sensitivity of the sensor was as high as 19.8 kPa^{-1}. However, when the pressure increased above 0.3 kPa, the sensitivity quickly decreased to only 0.27 kPa^{-1} (**Figure 9**A).

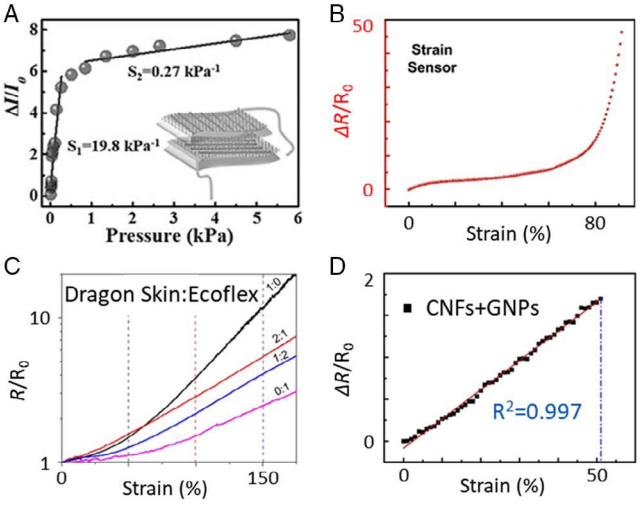

Figure 9. The types of resistance changes of SCCs with negative piezoresistivities during deformation. A) A pressure-sensing composite whose resistance decreases rapidly in the beginning of compression and then tends to stabilize (expressed by the current change through the sensor). Reproduced with permission.[137] Copyright 2017, Wiley-VCH. B) The resistance of a strain-sensing composite increases acceleratingly during stretching. Adapted with permission.[83] Copyright 2019, Wiley-VCH. C) The resistance of an electrical interconnection composite based on Dragon Skin-Ecoflex matrix that increases exponentially with strain. Adapted with permission.[8c] Copyright 2018, American Chemical Society. D) The resistance of an electrical interconnection composite, filled with CNF–graphite nanoplate (GNP) hybrid fillers, increases linearly with strain. Adapted with permission.[79] Copyright 2019, Elsevier.

Contrary to compression, the increase in resistivity accelerates for many composites during stretching as the strain increases. It is generally believed that under low tensile strain, although the conductive fillers are slightly separated and parts of the conductive paths are destroyed, the overall percolation network remains intact. However, under a large strain, most of the conductive paths are disconnected, and the remaining conductive paths are insufficient to maintain a percolation network, resulting in a sharp increase in resistivity (Figure 9B).[32,83] Through bending the layered conductive films, some researchers also indirectly compressed or stretched the conductive filler networks deposited on the film to study their piezoresistive properties.[55,81,138a] When bending, the outer surface of the film is stretched, whereas the inner surface is squeezed, with a strain proportional to the bending radius. By Monte Carlo simulation, a recent study analyzed the strain response of NW-filled conductive films under bending and

proposed some strategies to reduce the bending sensitivity of the films.[139]

Tunneling theory holds that the probability of electron tunneling between conductive fillers is inversely proportional to the power exponent of the distance between the fillers. According to this theory, the resistivity of the composite increases exponentially with tensile strain, which has been confirmed by many studies, especially composites filled with spherical particles (Figure 9C).[8b,c,22,35,94] However, one study found that when analyzing the strain response of some composites filled with spherical particles, the percolation model fits the experimental data better than the tunneling model.[129d] In addition, there are many composites with resistance that changes linearly with strain. These composites have a constant GF and are therefore ideal for applications as strain sensors (Figure 9D).[5a,79,89,140] However, there is also a contradiction between high strain sensitivity and high stretchability. High strain sensitivity is important for improving the sensitivity of sensors. However, the conductive networks of composites with high strain sensitivity are usually disconnected quickly during stretching, which limits their application in highly stretchable electronics.[56,89] Many studies sought to address this contradiction. Through the synergistic effect of hybrid fillers, researchers prepared a composite strain sensor with a GF of up to 13.1 while maintaining a wide elongation range of 300%.[7d] Another study reported a wearable strain-sensing textile based on 1D stretchable yarn sensors.[140] The as-prepared strain sensor not only exhibited high sensitivity with a GF of nearly 500 but also possessed a wide working range of 50% tensile strain.

4.2.3. Negative Piezoresistivity

Although contrary to common sense, several previous works have reported conductive composites with a negative piezoresistive effect. As the name suggests, the electrical resistance of these composites increases under compression (negative strain) but decreases when stretched (positive strain). Researchers proposed some theories to explain this unusual piezoresistive property, including the shear failure of the filler network during compression, the directional arrangement of fiber fillers or filler aggregates during stretching, and special composite structures.

Hybrid-filler composites with increased resistance during compression are generally filled with fillers such as CB, graphene, or CNTs. As mentioned previously, CB-filled composites simultaneously undergo the destruction and reconstruction of the CB conductive paths during compression. For some of them, the destruction of conductive paths dominates the resistance change during compression, resulting in a negative piezoresistive effect.[134,141] However, one study showed that after the instantaneous increase in resistance caused by compression, the separated CB particles tend to migrate together to form conductive paths. When the sample strain remained constant, the resistance decayed with time and gradually stabilized.[134] Graphene or CNT-filled hybrid-filler composite with negative piezoresistivity usually has low filler content. The contact resistance between these fillers with extremely high aspect ratios depends heavily on their mutual orientation. Therefore, their filler networks are prone to shear failure during compression and difficult to recover by forming new conductive paths, showing a negative piezoresistive effect (**Figure 10**A).[63,142,143] Generally, graphene-filled composites exhibit more significant negative piezoresistivity than CNT-filled composites. Take a PDMS-based SCC filled with graphene−Fe_3O_4 hybrid nanosheets as an example. When the concentration of graphene is slightly higher than its percolation threshold, the resistance of the composite increases exponentially by 870 times at a pressure of 0.88 MPa (Figure 10B).[144]

Hybrid-filler SCCs with increased conductivity during stretching usually use fiber as main fillers like metal NWs or CNTs. Although the sliding of the fibrous fillers during stretching slightly increases the contact resistance, the originally randomly oriented fibrous fillers slide along the elongation direction to rearrange. This directional alignment effect improves the conductivity of the composite during stretching (Figure 10C).[111] The resistance of the recently reported hybrid-filler stretchable conductive films filled with CNTs and polyaniline was reduced by 55% at a 100% tensile strain.[145] The narrow and long CB aggregates in silicone rubber composites can also orient along a direction like the fiber fillers. Therefore, these aggregates will also rotate and align during stretching due to the orientation effect, forming conductive paths to reduce the resistivity of the composites (Figure 10D).[141] In addition, prestretching and poststretching techniques can also produce composites with negative piezoresistivity. Through the prestrain or poststrain procedures, it is possible to deposit a tangled and oriented AgNW network on a transparent electrode[108] or form spring-structured CNTs in a PDMS matrix.[76b] During stretching, these filler structures extend in the elongation direction to form oriented structures, which significantly improve the electrical conductivity of these composites. Apart from earlier methods, some composites utilize special geometric structures to achieve negative piezoresistivity. For instance, a porous hybrid-filler SCC filled with CNTs and graphene exhibited a resistance reduction of 7.4% at 90% elongation due to the porous structure.[16a] Another recent study grew a wrinkled gold film on the surface of a conductive fiber. The gold film was flattened during stretching to reduce the electrical resistance of the conductive composite fiber.[92]

4.2.4. Strain-Insensitive SCCs

To develop composites for electrodes in stretchable electronics, many studies are devoted to the development of strain-insensitive conductive composites, whose resistance remains basically constant over a large range of strain. The most commonly used strategies are prestretching and poststretching methods. For example, using prestretching, methanol etching, and water vapor cold-welding techniques can greatly enhance the stretchability of the SCC film filled with CNTs−AgNWs hybrid fillers and reduce its strain sensitivity.[95] The composite film formed this way had a stable resistance stretched by 580%. Similar work also obtained a strain-insensitive conductive film by transferring metal-coated CNT tapes to a prestretched PDMS substrate.[113] Its resistance increased by 4% under a 100% tensile strain in the first cycle and remained stable in subsequent cycles (Figure 10E). Unlike most composites that can only maintain a stable resistance within the prestretched strain

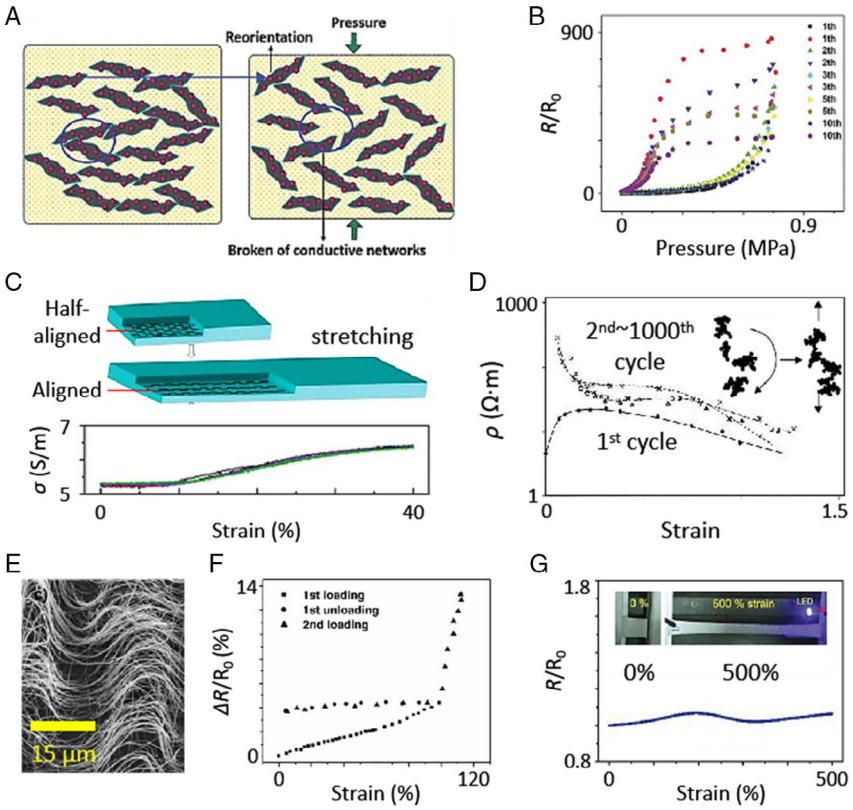

Figure 10. SCCs with positive piezoresistivities or insensitive to strain. A) The conductive network of a graphene-filled composite is sheared failure under pressure. B) The relative resistance—pressure curve of a graphene-filled composite with positive piezoresistivity. A,B) Reproduced with permission.[144] Copyright 2015, Wiley-VCH. C) The directional alignment effect of CNT fillers in an SCC during stretching and its conductivity–strain curve. Adapted with permission.[111] Copyright 2011, Royal Society of Chemistry. D) The resistivity–strain curves of a CB-filled composite under different stretching cycles. Inset shows the aggregates rotating and aligned during stretching. Adapted with permission.[141] Copyright 2003, Wiley Periodicals. E) SEM image and F) relative resistance change–strain curve of a prestretched CNT–PDMS conductive film. E,F) Adapted with permission.[113] Copyright 2012, Wiley-VCH. G) The relative resistance–strain curve of an LM-filled composite. The inset shows its photographs at 0% and 500% tensile strain. Adapted with permission.[147] Copyright 2019, Wiley-VCH.

range, one study reported a PDMS-based SCC film in which the substrate was only pre-stretched by 25%.[146] However, the composite film showed a stable conductivity at a 85% tensile strain. Similarly, another study fabricated composite conductor films with constant resistance up to 50% strain through the post-stretching method.[116d]

Using deformable LM as primary filler is another strategy.[26a] The LM droplets filled in an SCC can deform into a spindle shape during stretching to maintain the percolation network.[147] The resistance change of this composite was only 5% at a 500% tensile strain (Figure 10F). In addition, there are still many other methods for preparing SCCs with constant resistance under mechanical deformation. By adjusting the concentration of CNTs in the matrix, the destruction and reconstruction of the conductive paths during compression can be balanced.[11a] The as-prepared composite had a constant conductivity of 130 S m^{-1} in the compressive strain range of 0–13%. Likewise, adding AgNW auxiliary fillers can repair the defect conductive paths.[148] The strengthened hybrid-filler composite had a constant sheet resistance within 66% elongation. In addition, the porous aerogel structure can also impart the SCCs with constant resistance under strain.[72]

4.2.5. Special Piezoresistivity

Some composites exhibit opposite piezoresistive effects depending on the strain ranges during mechanical deformation, such as conductive composites filled with spiky-shaped nickel particles (SNPs). Due to the quantum tunneling effect, the electrical conductivity of these composites increases dramatically under any mechanical deformation, including compression, stretching, bending, and twisting (**Figure 11**A–C).[103,149] Therefore, these composites are also called quantum tunneling composites (QTCs).[150]

SNPs have sharp protrusions on the surface-like sea urchins (Figure 11D).[151] In the electric field (generated by the voltage decrease through the composite), the electric charge in the composite will generate local electric fields with high intensity at the tips of these protrusions. In the unstrained state, the distance between SNPs is too far to transfer charge, so the composite shows a high resistance. As the Poisson's ratio of most composites is much higher than 0, they will always be compressed in a certain direction under mechanical deformation. Unlike spherical fillers, the synapses on the surface of SNPs make them easy

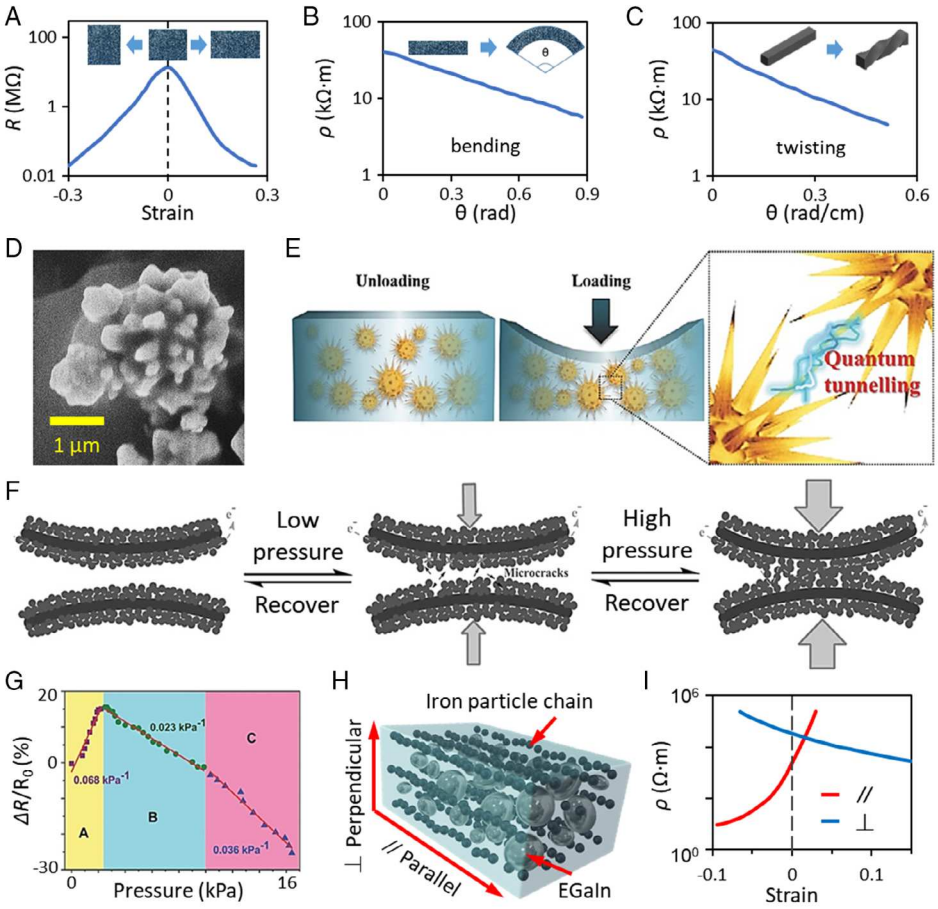

Figure 11. SCCs with special piezoresistivities. A) The resistance–strain curve of the LMMRE composite. B,C) The resistivity–strain curves of the LMMRE composite under B) bending and C) twisting. D) The SEM image of an SNP. A–D) Adapted under the terms of the CC-BY 4.0 license.[103] Copyright 2019, The Authors, published by Springer Nature. E) Schematic illustration of the electric field-assisted quantum tunneling effect of the composite filled with SNPs. Reproduced with permission.[151] Copyright 2016, Wiley-VCH. F) Schematic illustration of the conductive network changes of a conductive sponge with CB deposited on the surface under pressure. G) The relative resistance change–strain curve of this conductive sponge. F,G) Adapted with permission.[155] Copyright 2016, Wiley-VCH. H) Schematic image of the microstructure of an anisotropic conductive composite filled with Fe–EGaIn hybrid fillers. I) The resistivity–strain curves of this anisotropic conductive composite parallel and perpendicular to the alignment direction. H,I) Adapted with permission.[109a] Copyright 2020, Elsevier.

to contact with each other when the composite is deformed, which reduces the distance between the spikes of adjacent SNPs.[103] As a result, the quantum tunneling effect occurs as the probability of electron tunneling between adjacent particles increases exponentially when the thickness of the insulating layer between them decreases.[149] The high local electric field at the tips of SNPs further enhances this effect (Figure 11E).[151] Due to this electric field-assisted tunneling conduction, the resistance of composites filled with SNPs can be reduced by several orders of magnitude under a slight mechanical deformation. The resistance of a previously reported SNP–PDMS composite decreased by ten orders of magnitude at a 25% compressive strain or a 12% tensile strain.[149] Similarly, the resistance of another SNP-filled composite film can be reduced by six orders of magnitude at a bending radius of 6 mm.[152] However, the resistivity of the earlier composites in the unstrained state was usually as high as tens of MΩ·m, which severely limited their applications in electronics. To solve this problem, one group successfully reduced the electrical resistivity of SNP-filled composites to 70 kΩ·m by adding LM auxiliary fillers.[103] The electrical conductivity of the prepared composite increased significantly by 5 million times at a 10% compression or tensile strain. In addition, another study also presented a conductive composite filled with hybrid fillers of CBs and SNPs.[58] The synergistic effect of the hybrid fillers enhanced the conductivity of the composite and its long-term stability under compressive loading cycles but slightly reduced its strain sensitivity.

Contrary to the earlier QTCs with reduced resistance during deformation, the resistance of some composites increases significantly under any mechanical deformation. A CB-filled composite was reported, whose conductive network was easily disconnected under strain.[46b] This destruction effect dominates the strain response of the composite, resulting in an increase in several orders of magnitude in resistance under the compression or a tensile stress of 300 kPa.

In addition to the opposite strain response in the compression and stretching stages, some composites also exhibit opposite piezoresistive effects in different strain ranges during compression or stretching. The main reason for this phenomenon is that different factors dominate the strain response of the composites at different stages. For some composites, the directional arrangement of fillers and the tensile failure of the conductive paths take turns to dominate the resistance change. For example, the alignment of fiber fillers can cause the conductivity of composites to increase during stretching. Yet, after the elongation exceeds critical transition strain, an increasing number of filler conductive paths disconnect, and the conductivity rapidly declines.[52,153] In another study, the overall resistance of the AgNWs-filled conductive film increased when stretched but reduced during the 10–15% tensile strain range due to the alignment of the AgNWs.[154] As another example, a CB film deposited on the surface of a conductive sponge ruptures at the start of compression, which increases the resistance of the composite.[155] As the compressive strain increases, more adjacent branches contact each other, resulting in a reduction in the overall resistance (Figure 11F,G). In addition, the magnetic field-assisted alignment technique can create an anisotropic conductive composite filled with Fe MPs and EGaIn droplets.[109a] The Fe MPs are aligned into chain structures along the direction of the magnetic field and form a special anisotropic conductive network with the EGaIn droplets (Figure 11H). As a result, the piezoresistive properties of this composite changed with the measurement direction. It showed a conventional positive piezoresistivity along the particle alignment direction, but exhibited a negative piezoresistivity perpendicular to the alignment direction (Figure 11I). In a certain direction, the composite can even maintain a constant resistance under a low strain.

In summary, many numerical simulation methods and theories have been developed to describe the static and dynamic electrical properties of SCCs. However, there is still a lack of models and formulas that can accurately calculate the electrical conductivity of hybrid-filler composites. Depending on the types of fillers and elastomers and the processing methods, SCCs exhibit different piezoresistive effects. The in-depth analysis of the strain response of the composites will help researchers to further understand their conductive mechanism and develop applications that can take advantage of different piezoresistive characteristics.

5. Applications

The applications of hybrid-filler SCCs mainly depend on their electrical conductivity, stretchability, and strain response. This section summarizes their five main fields of application: stretchable electrodes and interconnects, sensors, actuators, special function composites, and stretchable electronic devices.

5.1. Stretchable Electrodes and Interconnects

5.1.1. Stretchable Electrodes

Stretchable electrodes and interconnects are the main applications of SCCs. As the important components of stretchable electronics, they require both high conductivity and high stretchability, which need composites that are insensitive or less sensitive to strain.[25b,28] In view of this, most hybrid-filler SCC electrodes or interconnects are filled with metal NWs[55,81a] or CNTs,[145] and their conductivity or stretchability is further enhanced by adding secondary fillers.[77,117,148] In addition, high long-term stability is also important to increase their service life.

The SCC electrodes are commonly used in stretchable electronic devices including resistive or capacitive flexible sensors, actuators, transistors, polymer batteries, etc.[25b,28] In a representative work, copper−silver core−shell NWs were used as fillers for transparent polyurethane electrodes. The silver shell outside the CuNWs enhanced the long-term stability of the electrode, which still exhibited a high conductivity after being stretched for 1000 times to a 30% strain.[94] Another study greatly improved the electrical conductivity of the electrode by plating a thin film of gold on the fiber fillers. The electrode had a sheet resistance as low as 7 $\Omega\,sq^{-1}$ at a 100% tensile strain and was used as a stretchable electrode grid implanted in vivo (**Figure 12**A,B).[8b] Using hybrid fillers of different types of fibers can simultaneously enhance the conductivity and stretchability of the electrode membrane. The electrode filled with CNT−AgNW hybrid fillers had a low sheet resistance of 10 $\Omega\,sq^{-1}$ at a 580% strain, which was used as the stretchable electrode of a dielectric elastomer actuator (DEA).[95] Using a hybrid network of long AgNFs and short AgNWs, it is possible to reduce the sheet resistance of a PDMS-based conductive film to only 1 $\Omega\,sq^{-1}$. The electrode not only had low piezoresistivity ($GF = 0.3$) but also could be stretched to a 70% strain by 15 000 times and therefore was used as the electrode of a capacitive fingerprint sensor (Figure 12C, D).[7e] In addition, bending resistance is also important for the electrodes in stretchable electronics. The resistance of most AgNW or CuNW electrodes increases rapidly after multiple bends; this problem can be solved by adding auxiliary fillers. Even after being bent by 10 000 times at a bending radius of 1 mm, the resistance of the AgNW electrode mechanically reinforced by nylon fiber remained constant, which provided advantages for its application in foldable polymer-dispersed liquid crystal films.[59] In previous research, LM-filled stretchable electrodes usually had an extremely high electrical conductivity and long-term stability. One group fixed the liquid gallium film to gold traces on a PDMS substrate through the formation of $AuGa_2$ alloy to fabricate flexible electrodes with a sheet resistance of only 0.5 $\Omega\,sq^{-1}$. Its resistance remained stable even after being stretched to a 50% strain one million times, exhibiting excellent electromechanical robustness.[117] By adding LM secondary fillers, the resistivity and strain sensitivity of an SCC electrode filled with silver flakes have been greatly reduced. The electrode had a conductivity of 8000 S cm^{-1} and could be repeatedly stretched to an 800% strain for more than 10 000 times, making it an ideal choice for electrodes in highly stretchable electronics.[36]

5.1.2. Stretchable Interconnects

Another application of SCCs with high conductivity and stretchability is making electrical interconnects. One study reported a conductive sponge filled with gold-plated graphene. The gold plating enhanced the electrical conductivity of the composite

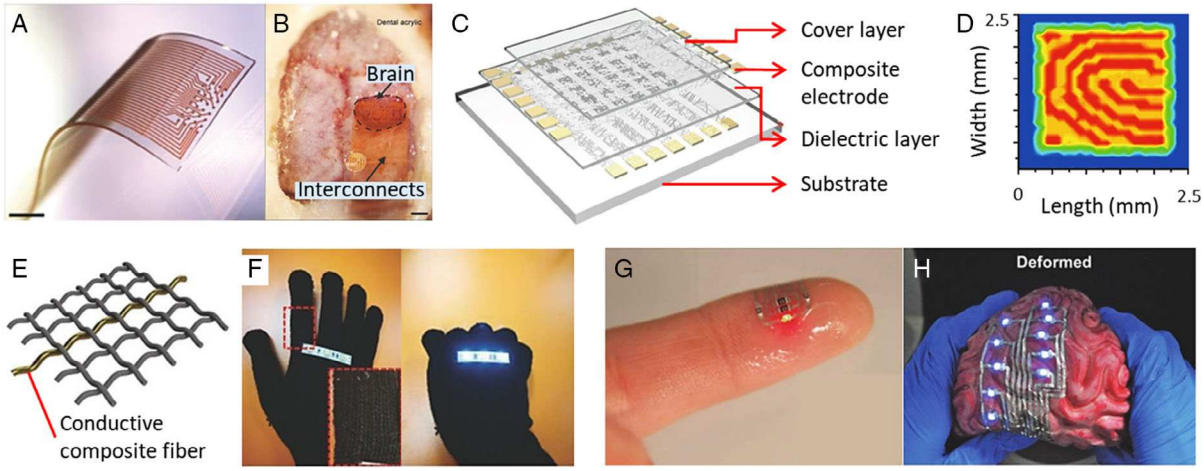

Figure 12. Applications of SCCs in stretchable electrodes and interconnects. A) Photograph of the soft stretchable electrode grids comprising gold-coated titanium dioxide NWs embedded in a silicone matrix. B) Intraoperative microphotograph of an implanted soft stretchable electrode grid for in vivo neural recording. Scale bar: 1 mm. A,B) Adapted with permission.[8b] Copyright 2018, Wiley-VCH. C) Schematic illustration of the fingerprint sensor structure. D) Captured 2 mm × 2 mm fingerprint pattern. C,D) Adapted under the terms of the CC-BY 4.0 license.[7e] Copyright 2018, The Authors, published by Springer Nature. E) The schematic illustration of a stretchable fiber conductor woven in a glove. F) Photographs of a conductive composite fiber woven in the finger area of a glove as a part of a wearable LED circuit. E,F) Adapted with permission.[92] Copyright 2018, Wiley-VCH. G) Electronic tattoo on human skin with an integrated LED on fingerprint. H) Deformable LED circuits on a soft model brain. G,H) Adapted with permission.[41] Copyright 2018, Wiley-VCH.

and prevented the conductive network from being disconnected under deformation. This conductive sponge with a low resistance and high stability could be used as a charging interconnect material for mobile phones.[8a] Similarly, a stretchable serpentine circuit is made of a conductive composite filled with silver-plated CuNWs. Even at 300% elongation, the LEDs in the circuit still worked normally (Figure 6C).[8c] Not all electrical interconnect composites have to be less sensitive to strain as long as they can maintain high conductivity during deformation. For instance, the sheet resistance of a conductive film filled with CNT–AgNW hybrid fillers increased by an order of magnitude at a 300% tensile strain. When used as the interconnect material in commercial LED array circuits, it could preserve a stable LED light intensity even at a 400% tensile strain due to its low initial resistance.[69] In another example, a gold-plated AuNW-filled fiber conductor was woven into a glove to act as the wire for wearable LED circuits (Figure 12E). It exhibited an increased electrical conductivity in a wide stretching range and therefore can work normally under severe deformations (Figure 12F).[92]

5.1.3. Conductive Ink

Compared with solid SCCs, conductive ink can be conveniently printed on any curved surface such as human skin and attached to the surface firmly. It can also be patterned by various printing techniques, demonstrating significant advantages in applications of electrodes and conductive interconnects.[84,86,100] In one work, the conductive ink filled with graphene and conductive CB hybrid fillers was processed into an electrode membrane by screen printing. This membrane electrode can withstand 100 000 stamping cycles and maintain electrical connection and was used as the electrode of piezoelectric sensors and dielectric elastomer transducers.[84] An EGaIn-reinforced AgNP conductive ink exhibits high conductivity (48 500 S cm^{-1}) and low strain sensitivity (GF ≈ 1). This ink can be printed on the human skin or a complex curved surface as deformable interconnects of microelectronic devices, which can maintain electrical connection over hundreds of loading cycles (Figure 12G,H).[41] Finally, in another study, a circuit printed with conductive ink filled with AgNPs and silver microsheets achieved a high conductivity of 935 S cm^{-1} at a high tensile strain of 400%. Based on this circuit, the researchers successfully developed a fully printed high-stretchable (up to 120%) sensor network for stretchable robots.[8d]

5.2. Stretchable Sensors

5.2.1. Sensitivity and Linearity of Sensors

SCCs with high piezoresistivities are promising materials for strain sensors. Compared with traditional rigid sensors, their main advantages are high flexibility and wide strain range.[1c,28] The sensitivity of strain sensors is generally evaluated by the GF. A previously reported PDMS-based conductive film sensor filled with AuNWs–AgNWs hybrid filler was extremely sensitive to strain (GF = 236.6). It had a strain resolution as low as 0.05% strain and therefore can detect small facial expressions and respiration vibrations. By increasing the number of layers of the conductive film, the sensitivity can be reduced and the stretchability can be improved.[56] Depositing a CNT–graphene hybrid layer on a microstructured PDMS film molded from natural leaves can prepare the conductive film with hierarchical protrusions. Then, two conductive films were placed face to face to construct a flexible pressure sensor (**Figure 13**A). Due to the unique hierarchical structure, the fabricated pressure sensor had a high

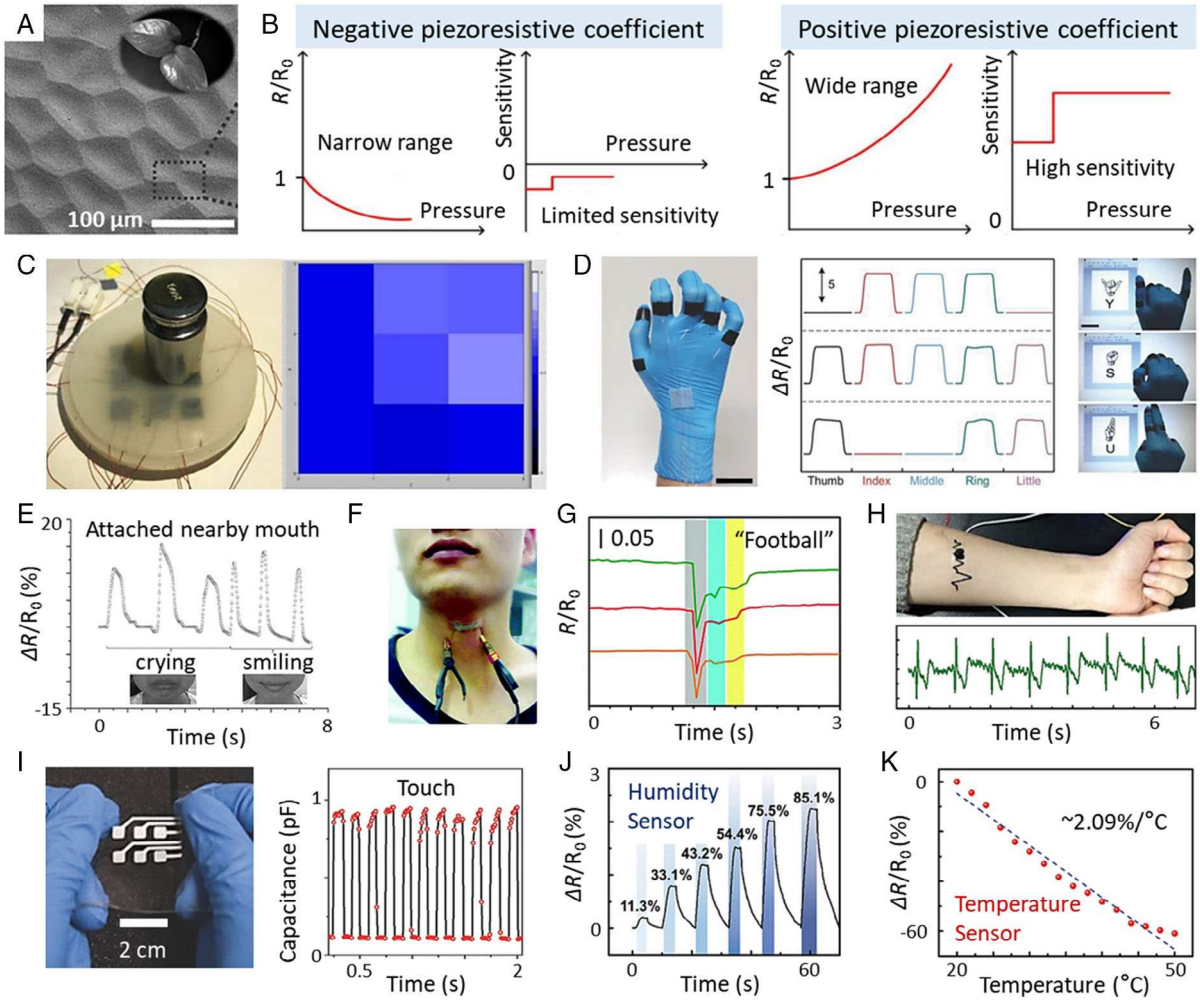

Figure 13. Applications of SCCs in stretchable sensors. A) SEM image of a patterned PDMS film molded from a leave (inset). The PDMS film is used as the substrate of a stretchable pressure sensor. Scale bar is 100 μm. Adapted with permission.[137] Copyright 2017, Wiley-VCH. B) The opposite pressure-sensing trends of piezoresistive sensors with a) negative and b) positive piezoresistive coefficients. C) Photograph of a 200 g weight placed on the pressure-sensing array with 3×3 pixels and the corresponding pressure distribution map. B,C) Adapted with permission.[142] Copyright 2020, American Chemical Society. D) Motion detection of English letters "Y," "S," and "U" for utilizing sign language glove. The composite fiber is attached to each finger of the glove. Scale bar: 3 cm. Adapted with permission.[74] Copyright 2015, Wiley-VCH. E) A transparent strain sensor is attached to skins near the mouth to sense expressions by time-dependent relative resistance change. Adapted with permission.[56] Copyright 2017, Wiley-VCH. F) Digital photograph of the electronic skin attached to the human neck to monitor the muscle motion during speech. G) Relative resistance–time curve for the electronic skin in response to voices saying "football." F,G) Adapted with permission.[157a] Copyright 2015, Royal Society of Chemistry. H) Photograph of an electronic tattoo directly attached on the forearm for electrocardiogram measurements and its relative resistance changes. Adapted with permission.[83] Copyright 2019, Wiley-VCH. I) Photograph of the patterned capacitive touch sensors and their capacitance change when the finger repeatedly touches the sensor surface. Adapted with permission.[36] Copyright 2018, Wiley-VCH. J,K) Performance of the electronic tattoo for monitoring the humidity and temperature. J) Real-time relative humidity sensing of the electronic tattoo at several relative humidity levels. K) Temperature sensing of the electronic tattoo from 20 to 50 °C. J,K) Adapted with permission.[83] Copyright 2019, Wiley-VCH.

sensitivity of 19.8 kPa^{-1} and a low detection limit of only 0.6 Pa. It also exhibited excellent stability over 35 000 compression cycles at 150 Pa.[137] Another study prepared a highly pressure-sensitive conductive film sensor for monitoring blood pressure by depositing CNT–graphene hybrid-filler composite NFs on a polymer substrate. Its resistance could be drastically reduced by six orders of magnitude at a pressure of 0.8 kPa.[64]

In addition to sensitivity, the high linearity of the resistance response to stress or strain is also important for stretchable sensors. Through dispersing graphene into the hydrogel matrix with the support of secondary fillers, a previous study prepared highly stretchable conductive hydrogels with linear strain response. In addition, a CNT–graphene hybrid-filler conductive film also shows a linear increase in resistance during stretching. However, the sensitivity of these two strain sensors was very low ($GF < 0.5$).[5a,75] Using the synergistic effect of carbon nanofibers (CNFs) and graphene fillers enhances the sensitivity and repeatability of PDMS-based SCCs. The wearable joint motion sensor

using such a composite maintained constant initial resistance after 1000 stretching cycles.[79] Adding AgNP secondary fillers to graphene-filled stretchable conductive yarns creates sensors with both high strain sensitivity (GF ≈ 500) and linearity (correlation coefficient = 0.98). Wearable and highly sensitive textile sensors woven with this yarn can monitor complex human movements such as gait and pronunciation.[140]

Compression sensors made of traditional positive piezoresistive SCCs have natural drawbacks, that is, they cannot achieve both high strain sensitivity and large measurement range at the same time. This is because the resistance of the positive piezoresistive composite can only be reduced to near zero at most when compressed. Assuming that the maximum compressive strain of the sensor is S_{max}, then the maximum GF is only $1/S_{max}$. In contrast, the sensitivity of composites with negative piezoresistivities will not be limited by the maximum strain because their resistance can increase unrestrictedly when compressed (Figure 13B). A recent study adjusted the piezoresistive properties of the CNTs-filled stretchable composite by adding silica NPs. At an appropriate filler content, the composite had a linear negative piezoresistivity, exhibiting a high sensing range of 175 kPa (≈60% compressive strain) and high sensitivity (≈0.1 kPa^{-1}). This composite showed successful applications in grip- and gait-sensing and pressure-sensing arrays (Figure 13C).[142] Likewise, another group reported a high-negative-piezoresistive conductive composite filled with graphene−Fe_3O_4 hybrid sheets. Its electrical resistance increased sharply by three orders of magnitude at 23% compressive strain, showing potential applications in wearable pressure sensors.[144]

5.2.2. Stress and Strain Sensors

Due to comprehensive research on the piezoresistive properties of SCCs, their applications in sensors are mostly stress or strain sensors. Most 2D or 3D composite sensors are designed to sense compression or stretching, whereas 1D conductive yarns can additionally be developed into bending and torsion sensors.[87,156] With significantly higher stretchability and flexibility than traditional rigid sensors, these flexible sensors are used as wearable devices for real-time health monitoring. They can detect almost all human signals that cause deformations, including but not limited to human joint movement,[7d,75,79] touch,[36,144] blood pressure,[64] and weak muscle movements (such as facial expressions, respiration, heart rate, pulse, vocal cord vibration, chewing, and swallowing).[56,83,97,98,157]

Most joint motion sensors are installed outside the bendable joint to sense the bending angle through the tensile strain generated during bending. This requires high mechanical stretchability of the composite because the sensor patch on the finger or elbow joint may produce a strain up to 200% when bent. A previously reported CNT−PDMS composite whose conductivity was enhanced by CB secondary fillers showed a tensile limit of 300% and excellent long-term stability during stretching cycles (2500 cycles at a 200% strain). Harnessing the superb sensing performances, these stretchable sensors were attached onto different human joints to develop the large human motions detection system.[7d] Another study presented hybrid-filler conductive yarns with high fracture strain (1250%) and electrical conductivity (13 S cm^{-1}). These yarns could be woven into a wearable joint motion-sensing textile.[11b] The joint sensors were commonly used to monitor finger movements. Using a hybrid-filler conductive film that can be stretched by 80%, researchers made a motion-sensing glove that can simultaneously monitor the bending of five fingers.[35] Similarly, a smart glove for detecting sign language has been demonstrated by embedding highly stretchable SCC fibers in the glove (Figure 13D).[74]

Unlike joint motion sensors that are subject to large strains, touch sensors and blood pressure sensors have to respond to tiny pressures and therefore require high strain sensitivity. One typical example is the aforementioned graphene−Fe_3O_4 hybrid-filler composite for touch sensor and the conductive film for blood pressure monitoring.[64,144] Some high strain-sensitive skin sensors are used in real-time healthcare monitoring by detecting weak muscle movements. These sensors attached to the skin surface usually have a very low Young's modulus and thus can detect tiny skin deformations caused by respiration, pulse, vocal cord vibration, or facial expressions.[157b] The "invisible" wearable sensor developed with a transparent stretchable conductive film with high positive piezoresistivity can distinguish different expressions like crying and smiling (Figure 13E).[56] By plating silver on the surface of CuNW fillers to obtain antioxidation ability, it is possible to enhance the sensitivity and response speed of an electronic skin sensor. In addition to monitoring human pulse, this electronic skin can even achieve rough voice recognition by sensing the muscle motion during speech (Figure 13F.G).[157a]

Furthermore, some researchers also printed functional circuits with conductive inks to sense strain.[117] For instance, a wearable electromyogram sensor can be printed onto a textile garment using the highly conductive silver sheets-filled ink. The sensor attached to the forearm could recognize the opening and closing of the hand.[34] Compared with the polymer skin sensor, the functional circuit printed directly on the human skin, also known as electronic tattoo, can perform high-fidelity strain sensing. One group reported a repairable multifunctional electronic tattoo filled with graphene. Due to its high strain fidelity and sensitivity, the monitored electrocardiogram could even be comparable with professional medical instruments (Figure 13H).[83]

In addition, some SCCs also undergo capacitance changes when deformed, which can also be used to sense strain.[25b,87,158] Multilayered coaxial stretchable conductive fibers made by layering CNTs and rubber polymers on a prestretched polymer core exhibit approximately linearly increasing capacitance during stretching, which can be used as capacitive strain sensors.[76a] Two LM-filled stretchable conductive fibers twisted into a spiral can sense torsion, touch, and stretching through capacitance changes caused by geometric deformation.[156a] In addition to conductive fibers, printing conductive ink on the substrate can also prepare capacitive touch sensors. The principle is that the contact between the finger and the touch sensor will parallel the initial capacitance of the sensor with the capacitance of the human body, thereby increasing the total capacitance (Figure 13I).[36]

5.2.3. Other Types of Sensors

The resistance of some conductive composites is not only sensitive to the mechanical deformation, other physical or chemical

signals may also affect their resistance, such as temperature, magnetic field, light intensity, humidity, and odor molecule concentration.[4c,8d,83,103,138] Harnessing these unique properties, a variety of sensors for sensing physical and chemical signals have been developed. For example, the aforementioned graphene-filled electronic tattoo could respond to environmental changes, including temperature and humidity, and therefore was used as a stable temperature and humidity sensor (Figure 13J,K).[83] Some SCCs filled with ferromagnetic particles such as iron and nickel are sensitive to magnetic fields. A previously reported composite filled with iron MPs and EGaIn droplets showed a resistance reduction of 55% at a magnetic field strength of 0.2 T.[103] In another work, conductive ink filled with CNTs and graphene was printed on a paper–polymer bilayer film to create a sensor that responds to changes in light irradiation and relative humidity. During illumination, the hybrid film absorbed photons to generate heat and bend, resulting in a reduction in resistance.[138]

5.3. Stretchable Functional Actuators

Another common application for SCCs is the function actuator. The function actuator mentioned here refers to relying on the composite itself to perform functions such as heating or actuation, rather than just using it as an electrode of the actuator. The heaters developed by SCCs are generally resistance heaters, which generate heat by the Joule heating effect when the composites are energized. Compared with the traditional resistance wire heater, the stretchable heater not only can withstand large deformations such as bending and stretching but also has high workability and adaptability. It can work on curved surfaces such as human limbs and be processed into any shape to meet different requirements (**Figure 14**A).[26a,103,117] In addition, some studies also reported on transparent SCC heating films filled with conductive fibers.[55,94,120] Most SCC heaters have a relatively stable resistance under strain, which can ensure that their heating efficiency will not change drastically under mechanical deformations. A previously reported LM-filled stretchable resistance heater showed constant resistance under a tensile strain of 700%, thereby maintaining a stable output power.[26a] However, not all composite heaters are insensitive to strain. Take an intelligent heating film based on the aforementioned LMMRE as an example. As the composite had an extreme high initial resistance and can significant decrease its resistance under any mechanical deformation, the heating film made from LMMRE worked

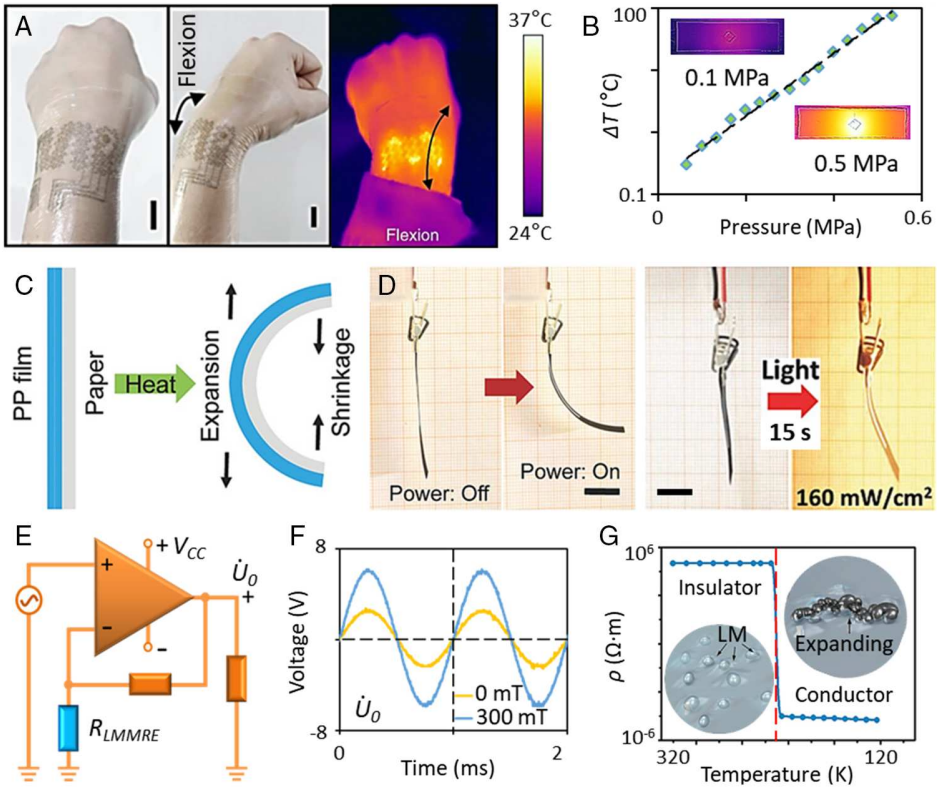

Figure 14. Applications of SCCs in stretchable function actuators. A) Optical camera image and infrared camera image of the wearable heating electronic patch on a wrist. Scale bar: 2 cm. Adapted with permission.[22] Copyright 2018, Springer Nature. B) The temperature change–pressure curve of the LMMRE heating film. Adapted under the terms of the CC-BY 4.0 license.[103] Copyright 2019, The Authors, published by Springer Nature. C) Mechanism diagram of the paper-polymer bilayer actuator. D) Bending deformation of an actuator upon application of 30 V or light irradiation. Scale bar: 1 cm. C,D) Adapted under the terms of the CC-BY 4.0 license.[138] Copyright 2018, The Authors, published by Wiley-VCH. E,F) Diagram and actual output signals for the LMMRE-based AC signal amplification circuit. Adapted under the terms of the CC-BY 4.0 license.[103] Copyright 2019, The Authors, published by Springer Nature. G) The resistivity–temperature curve of the LM-filled switch conductor. Inset shows the mechanism diagram of the electrical transition between insulating and conducting states in response to temperature changes. Adapted with permission.[147] Copyright 2019, Wiley-VCH.

under surface pressure or stretching. According to different surface pressures, it could automatically adjust the heating power, reflecting its potential in smart wearable heaters (Figure 14B).[103]

SCCs can also be developed to make actuators controlled by electric field, magnetic field, temperature, or light.[20,76,138a] High-stroke torsional fiber muscles can be fabricated with twisted SCC fibers. The torsional fiber muscles controlled by electric field can achieve tensile drive and torsional drive.[76a] Taking advantage of the difference in the thermal expansion coefficients of paper and polymer, the paper−polymer bilayer film with a hybrid-filler conductive ink printed on the surface realized bending actuation controlled by voltage, temperature, and light intensity (Figure 14C,D).[138] By adding the secondary filler of ferromagnetic particles, the conductive hydrogel can be bent in the magnetic field generated by a bar magnet to switch the circuit remotely.[20] In addition, conductive composites can also be used as luminescent materials. A previous study filled the composite with ZnS:Cu particles to develop alternating current (AC) electroluminescent devices.[19]

As the resistance of SCCs could be easily controlled by surface pressure or other physical and chemical signals, these composites were also used as controllers for signal amplification circuits or circuit switching materials. A recent study integrated the fabricated LMMRE into an operational amplifier AC signal amplification circuit. The signal amplification factor of the circuit could be adjusted by changing the surface pressure or magnetic field strength on the composite (Figure 14E,F).[103] In another work, a thermally sensitive conductive composite filled with SNPs and graphene showed a sharp increase in resistance when the temperature increased, and thus this was used as a thermal safety switch for batteries.[159] Using the contact conduction caused by the volume expansion of LM during solidification, a recent study made a temperature-controlled switch conductor filled with LM droplets. When the temperature of the switch conductor exceeds the melting point of the LM, its resistance can be increased by nine orders of magnitude instantaneously, thereby achieving a step temperature response without transition (Figure 14G).[147] In addition, some hybrid-filler conductive sponges were also used as pressure-sensitive switch materials due to their extremely high sensitivity, fast response, and excellent repeatability.[70,97,160]

5.4. Special Functional Composites

In addition to the aforementioned applications, some hybrid-filler SCCs also have many unique and interesting functions. Stretchable electromagnetic interference (EMI)-shielding material is a relatively mature application among them. The EMI-shielding hybrid-filler composites absorb or shield electromagnetic waves by the high-concentration conductive filler percolation network and usually have a high electrical conductivity. Most of them also have a low strain sensitivity to preserve stable EMI shielding effectiveness (SE) during mechanical deformations. The role of the auxiliary filler in these composite is to disperse the main fillers or produce a synergistic effect with them to strengthen the percolation network and enhance the conductivity.[7c,31,161] There are two types of commonly used fillers: metals (silver, nickel, copper, etc.) and carbon fillers (CNT, graphene, CB).[3b,31,68a,73b] A recent study prepared a stretchable EMI-shielding composite with an EMI SE of 57.1 dB through the synergistic effect of silver and nickel NPs. It showed an excellent EMI-shielding effect even after 10 000 stretching cycles at a 100% tensile strain.[31] Another study reported a hybrid-filler EMI-shielding composite filled with magnetic cobalt and polyaniline particles. The microwave absorption frequency of this composite can be adjusted by the ratio of the two fillers, showing an application prospect in the frequency-adjustable EMI-absorbing material.[162]

Some SCCs achieve self-healing relying on special fillers or elastomers. After being broken or cut, these materials can restore the mechanical and electrical connection. Generally, this is achieved by a macromolecular polymer matrix with self-healing function. When the two cross sections of the composite are attached, the macromolecular chains in the polymer will be reconnected through physical or chemical bonds to repair the composite and restore electrical conductivity to a certain extent.[83,118,163] Some recent researches have also developed composite conductive inks based on LM, which can form self-healing conductive traces in stretchable electronics.[7a,100] A recent study printed an iron particle−EGaIn composite conductive ink on a polymer substrate to form a magnetic self-healing circuit. When the circuit was damaged, the iron powder in the ink was attracted by the magnet to drive the EGaIn and repair the circuit (**Figure 15**A).[100] Another study injected the LM−PDMS ink within the crevices of severely damaged wires and assembled LM microdroplets by dielectrophoresis to form stretchable microwires that can heal the damage mechanically and electrically.[164] Combining self-healing elastomers with LM can create a self-healing SCC comprising nickel flakes, EGaIn, and carboxylated polyurethane (CPU). When the composite is damaged, EGaIn can flow to connect the nickel flakes and repair the conductive network, and the CPU can achieve mechanically healing through the interfacial hydrogen bonding. After being healed at room temperature for 1 h, the repaired composite retained a fracture strain of 100% and recovered 75% of the initial conductivity (Figure 15B).[21]

Recyclable conductive composites are another interesting functional material. The recyclable circuit can be manufactured by printing LM-based SCC ink on a hydrolyzable substrate. This circuit can be dissolved in water to recover the LM (Figure 15C,D).[100] Doping amorphous calcium carbonate filler can also prepare recyclable hybrid-filler conductive composites. These composites were hard when dry and became deformable and remodelable when wet, showing recyclability. In addition, the gel-like composite in the wet state can also be used as the 3D printing silk material to be processed into various shapes.[163] Similarly, the mixture of conductive fillers and liquid elastomers like PDMS or Ecoflex can also be used as the silk material for 3D printing. These liquid materials are cured and shaped during the 3D printing process to obtain conductive composites with complex geometries (Figure 15E,F).[142]

Using different combinations of fillers and matrices and fabrication methods, conductive composites have been developed with functions such as shape memory (Figure 15G),[20,73a] catalysis,[24b,165] liquid crystal display,[59] cell compatibility,[51a,166] antibacterial,[23] and water and oil resistance.[88] With the further deepening of research on SCCs, it is believed that conductive

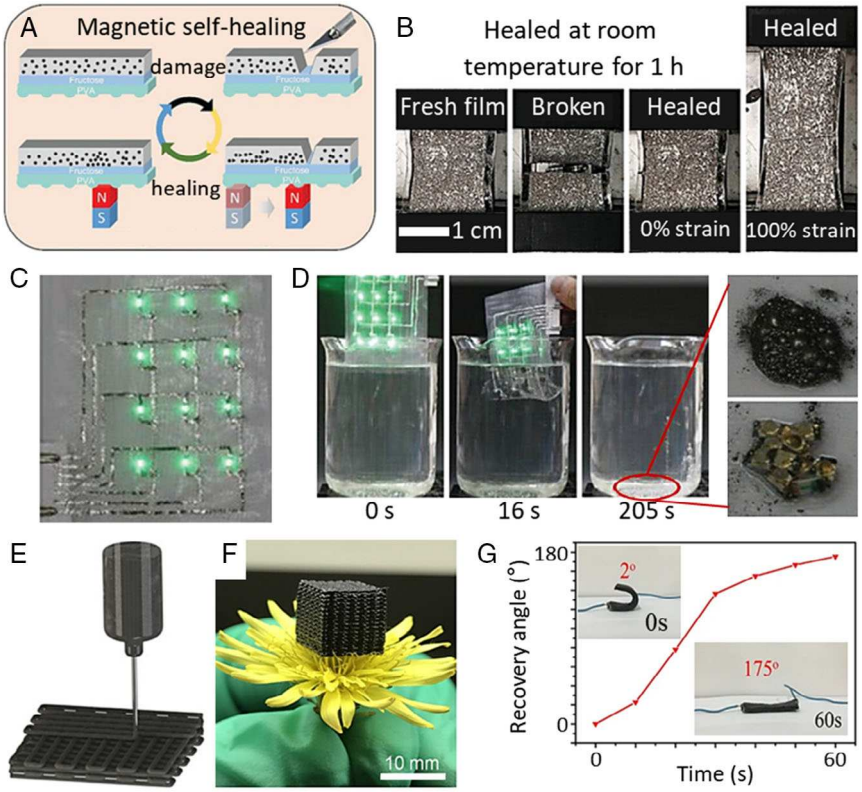

Figure 15. Applications of SCCs with special functions. A) Schematic illustration of the healing process of Fe−EGaIn circuit using magnetic field. Adapted under the terms of the CC-BY 4.0 license.[100] Copyright 2019, The Authors, published by Wiley-VCH. B) Photograph of the Ni–EGaIn–CPU conductor before and after breaking and the healed conductor under 0% and 100% tensile strain. Adapted with permission.[21] Copyright 2019, Wiley-VCH. C) Photograph of recyclable LED array based on the LM and hydrolyzable substrate. D) The dissolution and recycle process of the recyclable LED array. C,D) Adapted under the terms of the CC-BY 4.0 license.[100] Copyright 2019, The Authors, published by Wiley-VCH. E) Schematic illustration of the 3D printing process for manufacturing the pressure sensor with complex geometries. F) Photograph of a 3D-printed pressure sensor on a flower. E,F) Adapted with permission.[142] Copyright 2020, American Chemical Society. G) The recovery angle–time curve of the shape recovery process of a shape memory composite under voltage of 40 V. Insets show the photographs of the shape memory composite at 0 and 60 s during the shape recovery process. Adapted under the terms of the CC-BY 4.0 license.[73a] Copyright 2017, The Authors, published by Springer Nature.

composites with more complex and novel functions will be developed in the future.

5.5. Stretchable Electronic Devices

The stretchable electronic devices can be fabricated by combining stretchable components with different functions. The electrodes, circuits, or functional electronic components such as sensors and actuators in these electronic devices are all SCCs. Without rigid components, these intrinsically stretchable electronic devices show significant advantages in soft robots and wearable applications.[1c,d,28]

One of the most common stretchable electronic devices is the stretchable sensor, usually composed of a sensor composite and an electrode or interconnected composite with a low strain sensitivity.[84,85,98a] For instance, a previous work combined a conductive ink-printed circuit with a nickel-filled pressure-sensitive composite to develop fully printed stretchable pressure-sensing networks on a glove (**Figure 16**A,B).[8d] By combining composite electrodes with functional conductive materials, some functional actuators such as DEAs,[95,117] electroluminescent composites,[19] electrochromic composites,[81a] and stretchable field-effect transistors (FETs)[34,102] have been developed. Encapsulating electroluminescent particle-filled composites with AgNW−PDMS stretchable electrodes can prepare stretchable electroluminescent devices (Figure 16C,D).[19] By adding different hybrid fillers into the PDMS base, researchers prepared stretchable composite semiconductors (filled with CNTs and polymer NFs) and composite electrodes (filled with AuNPs and AgNWs). Then, the two composites were combined to form a stretchable rubbery FET array, and its application as the tactile sensing skin was shown.[102]

A major difficulty for the application of stretchable electronic devices is the source of power. Using an external power supply will limit their application scenarios, whereas the use of battery power is not conducive to their flexibility. Therefore, it is very important to develop energy-conversion and collection devices based on stretchable composite components.[28] A highly stretchable triboelectric nanogenerator (HS-TENG) was developed using SCC yarns as the negative electrode and a nylon-coated nickel−copper flexible fabric as the positive electrode. This

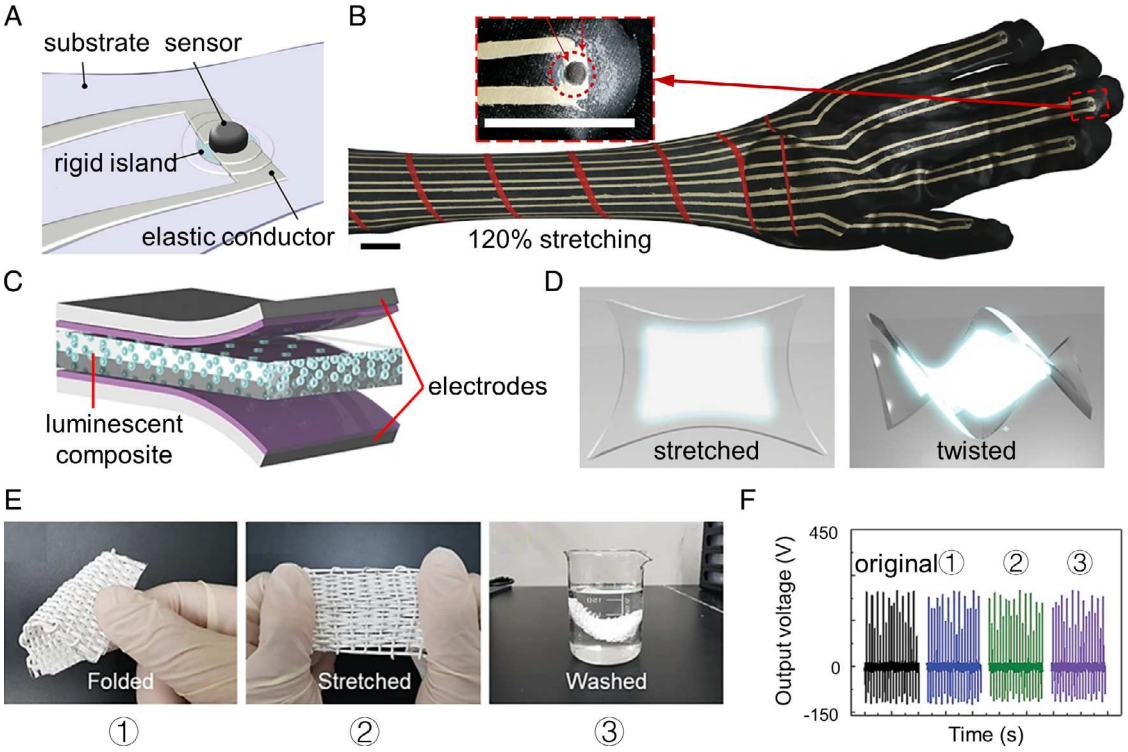

Figure 16. Applications of SCCs in stretchable electronic devices. A) Structure of sensors networks. Sensors are placed on printed polyurethane islands and wired using the conductive ink. B) Photograph of sensor networks under 120% tensile strain. Inset shows a magnified image of a sensor. Scale bar: 2 cm. A,B) Adapted with permission.[8d] Copyright 2017, Springer Nature. C) Schematic image of the electroluminescent device geometry. D) Schematic images of the electroluminescent device under stretching and twisting. C,D) Adapted with permission.[19] Copyright 2015, Wiley-VCH. E) Photographs of the TENG under three different extreme conditions: folding, stretching, and washing. F) Output voltages of the TENG after experiencing extreme conditions. E,F) Adapted with permission.[101] Copyright 2019, Wiley-VCH.

HS-TENG preserves stable output power under various extreme conditions, such as folding, twisting and washing, demonstrating promising applications as the power sources for wearable stretchable electronics (Figure 16E,F).[101]

6. Conclusion and Outlook

In recent years, SCCs have shown promise for stretchable electronics, soft robots, and wearable devices. In general, their applications depend on the response of their electrical resistance to mechanical deformation. Therefore, an in-depth analysis of the strain response of these composites is very helpful to understand their conductive mechanism and develop new applications. Around this point, this Review introduces and analyzes the fabrication process, stretchable design, static and dynamic conductivity analysis, and recent applications of SCCs, with emphasis on composites filled with hybrid fillers.

Many composites include secondary fillers to improve their physical or chemical properties, such as electrical and thermal conductivity, dielectric properties, mechanical strength, stability, oxidation resistance, and antibacterial properties. For hybrid-filler SCCs, secondary fillers are mainly used to enhance the conductivity, stretchability, or repeatability under cyclic loading. Sometimes they can also adjust the strain sensitivity of the electrical conductivity. There are three main types of conductive fillers: metal fillers, carbon fillers, and CPs. Although the metal filler has high conductivity, it will significantly reduce the flexibility and mechanical stretchability of the composite and is easy to oxidize. In comparison, carbon-based fillers are chemically stable and hard to corrode, but they are difficult to disperse evenly in the matrix and have low electrical conductivity. CP fillers show the advantage in stretchability, but also have low electrical conductivity. Conventional single-filler conductive composites usually have limited functions and encounter one of the earlier limitations. In contrast, the hybrid-filler composites can combine the advantages of different fillers to eliminate these disadvantages to a certain extent. However, improper filler combination and ratio may damage the conductive percolation network, so the appropriate matching of hybrid fillers is very important.

Although hybrid fillers impart conductive composites with excellent electrical or mechanical properties, they also greatly increase the difficulty of numerical simulation of the electrical conductivity. Hybrid fillers have different shapes and sizes and complex percolation networks, so it is difficult to derive a general conductivity formula. Their conductivity simulations

generally rely on Monte Carlo statistical experimental methods. Many theories have been proposed to explain the conductivity change of SCCs under mechanical deformations. Depending on the filler geometry and fabrication methods, conductive composites exhibit a variety of piezoresistivities, including positive piezoresistivity, negative piezoresistivity, strain insensitivity, and special piezoresistivity, which directly determine their application fields. Conductive composites with stable resistance during stretching are mainly used as electrodes and interconnects in electronic devices. Stress and strain sensors are mostly developed with composites with linear piezoresistivities. Some hybrid-filler conductive composites also show additional functions such as self-healing, shape memory, recyclability, antibacterial, and catalysis, to name a few. By assembling different types of SCCs, various electronic devices have been developed. These stretchable electronics exhibit attractive applications in the fields of flexible sensors and actuators, wearable heating and energy-harvesting devices, and human healthcare monitoring.

However, it should be acknowledged that the linearity and long-term operating stability of current stretchable composites are inferior to mature commercial sensors and other electronics. For the detection of physical quantities other than strain and pressure (such as temperature, humidity, and magnetic field), the resolution, accuracy, dynamic range, and long-term stability of SCC sensors are generally lower than that of commercial counterparts. The service life of SCC-based electronic devices, such as SCC heating films, may also be lower than that of commercial products made from resistive patches with embedded heating wires. In addition, the processing accuracy and resolution of SCCs are generally low, making them difficult to be applied in the field of microelectronics for manufacturing integrated circuit boards. Therefore, it is still impractical for SCCs to fully replace the role of rigid conductive materials at present. To this end, future research may focus more on the design and manufacturing of SCCs with superior properties and novel functions, such as solid−liquid phase conversion, corrosion resistance, abrasion resistance, high compressibility, and unique piezoresistivity.

Acknowledgements

S.-Y.T. is grateful for the support from the Royal Society (IEC\NSFC\201223). M.D.D. is grateful for the support from the National Science Foundation (ASSIST, EEC-1160483, and CMMI- 2032409).

Conflict of Interest

The authors declare no conflict of interest.

Keywords

conductive composites, hybrid fillers, stretchable composites, stretchable electronics

Received: December 29, 2020
Revised: April 6, 2021
Published online:

[1] a) J. A. Rogers, T. Someya, Y. Huang, *Science* **2010**, *327*, 1603; b) B. C. K. Tee, J. Ouyang, *Adv. Mater.* **2018**, *30*, 1802560; c) D. C. Kim, H. J. Shim, W. Lee, J. H. Koo, D.-H. Kim, *Adv. Mater.* **2020**, *32*, 1902743; d) Y. Liu, K. He, G. Chen, W. R. Leow, X. Chen, *Chem. Rev.* **2017**, *117*, 12893.

[2] a) T. Cheng, Y. Zhang, W.-Y. Lai, W. Huang, *Adv. Mater.* **2015**, *27*, 3349; b) H. Joo, D. Jung, S.-H. Sunwoo, J. H. Koo, D.-H. Kim, *Small* **2020**, *16*, 1906270.

[3] a) S. Paszkiewicz, A. Szymczyk, I. Kasprowiak, M. Zenker, R. Pilawka, A. Linares, T. A. Ezquerra, Z. Rosłaniec, *Polym. Compos.* **2018**, *39*, 2961; b) R. Ravindren, S. Mondal, K. Nath, N. C. Das, *Polym. Adv. Technol.* **2019**, *30*, 1506; c) Z.-F. Sun, P.-G. Ren, Z.-W. Zhang, F. Ren, *J. Appl. Polym. Sci.* **2019**, *136*, 47317.

[4] a) Y. Wang, J. Chen, Y. Shen, T. Wang, Y. Ni, Z. Zhang, L. Sun, B. Ji, B. Wang, *Polymer Engineering & Science* **2019**, *59*, E224; b) R. Liu, Y. Chen, Q. Ma, J. Luo, W. Wei, X. Liu, *J. Appl. Polym. Sci.* **2017**, *134*; c) K. Guo, D.-L. Zhang, X.-M. Zhang, J. Zhang, L.-S. Ding, B.-J. Li, S. Zhang, *Angew. Chem. Int. Ed.* **2015**, *54*, 12127; d) S. Li, Z. Wang, J. Jia, C. Hou, X. Hao, H. Zhang, *Polym. Compos.* **2018**, *39*, 1212.

[5] a) Q. Wang, L. Li, Z. Lu, X. Hu, Z. Li, G. Sun, *ChemElectroChem* **2019**, *6*, 5006; b) Y. Huang, W. Wang, X. Zeng, X. Guo, Y. Zhang, P. Liu, Y. Ma, Y. Zhang, *J. Appl. Polym. Sci.* **2018**, *135*, 46517; c) M. G. Jang, S. C. Ryu, K. J. Juhn, S. K. Kim, W. N. Kim, *J. Appl. Polym. Sci.* **2019**, *136*, 47302; d) I. C. Kim, K. H. Kwon, W. N. Kim, *J. Appl. Polym. Sci.* **2019**, *136*, 48162.

[6] a) A. Krainoi, C. Kummerlöwe, Y. Nakaramontri, S. Wisunthorn, N. Vennemann, S. Pichaiyut, S. Kiatkamjornwong, C. Nakason, *Polym. Compos.* **2020**, *41*, 443; b) A. Krainoi, C. Kummerlöwe, N. Vennemann, Y. Nakaramontri, S. Pichaiyut, C. Nakason, *J. Appl. Polym. Sci.* **2019**, *136*, 47281.

[7] a) M. G. Saborio, S. Cai, J. Tang, M. B. Ghasemian, M. Mayyas, J. Han, M. J. Christoe, S. Peng, P. Koshy, D. Esrafilzadeh, R. Jalili, C. H. Wang, K. Kalantar-Zadeh, *Small* **2020**, *16*, 1903753; b) F. Zhang, Y. Feng, M. Qin, L. Gao, Z. Li, F. Zhao, Z. Zhang, F. Lv, W. Feng, *Adv. Funct. Mater.* **2019**, *29*, 1901383; c) S. Zhu, C. Xing, F. Wu, X. Zuo, Y. Zhang, C. Yu, M. Chen, W. Li, Q. Li, L. Liu, *Carbon* **2019**, *145*, 259; d) Y. Zheng, Y. Li, K. Dai, Y. Wang, G. Zheng, C. Liu, C. Shen, *Compos. Sci. Technol.* **2018**, *156*, 276; e) B. W. An, S. Heo, S. Ji, F. Bien, J.-U. Park, *Nat. Commun.* **2018**, *9*, 2458.

[8] a) F. Han, X. Su, M. Huang, J. Li, Y. Zhang, S. Zhao, F. Liu, B. Zhang, Y. Wang, G. Zhang, R. Sun, C.-P. Wong, *J. Mater. Chem. C* **2018**, *6*, 8135; b) K. Tybrandt, D. Khodagholy, B. Dielacher, F. Stauffer, A. F. Renz, G. Buzsáki, J. Vörös, *Adv. Mater.* **2018**, *30*, 1706520; c) M. J. Catenacci, C. Reyes, M. A. Cruz, B. J. Wiley, *ACS Nano* **2018**, *12*, 3689; d) N. Matsuhisa, D. Inoue, P. Zalar, H. Jin, Y. Matsuba, A. Itoh, T. Yokota, D. Hashizume, T. Someya, *Nat. Mater.* **2017**, *16*, 834.

[9] a) X.-J. Zha, J. Yang, J.-H. Pu, C.-P. Feng, L. Bai, R.-Y. Bao, Z.-Y. Liu, M.-B. Yang, W. Yang, *Adv. Mater. Interfaces* **2019**, *6*, 1900081; b) K. Raza, M. U. Siddiqui, A. F. M. Arif, S. S. Akhtar, A. S. Hakeem, *Polym. Compos.* **2019**, *40*, 1419; c) T. Lu, H. Ye, A. Zheng, X. Xu, C. Xu, H. Wang, L. Sun, L. Xu, *J. Appl. Polym. Sci.* **2017**, *134*, 44848; d) M. I. Ralphs, N. Kemme, P. B. Vartak, E. Joseph, S. Tipnis, S. Turnage, K. N. Solanki, R. Y. Wang, K. Rykaczewski, *ACS Appl. Mater. Interfaces* **2018**, *10*, 2083; e) R. Bao, S. Yan, R. Wang, Y. Li, *J. Appl. Polym. Sci.* **2017**, *134*, 45555; f) Z. Wu, C. Xu, C. Ma, Z. Liu, H.-M. Cheng, W. Ren, *Adv. Mater.* **2019**, *31*, 1900199; g) J.-U. Jang, H. C. Park, H. S. Lee, M.-S. Khil, S. Y. Kim, *Sci. Rep.* **2018**, *8*, 7659.

[10] a) A. Naji, B. Krause, P. Pötschke, A. Ameli, *Polym. Compos.* **2019**, *40*, 3189; b) Q. C. Tan, R. A. Shanks, D. Hui, I. Kong, *Composites Part B* **2016**, *90*, 315.

[11] a) F. Schütt, S. Signetti, H. Krüger, S. Röder, D. Smazna, S. Kaps, S. N. Gorb, Y. K. Mishra, N. M. Pugno, R. Adelung, *Nat. Commun.* **2017**, *8*, 1215; b) Y. Li, B. Zhou, G. Zheng, X. Liu, T. Li, C. Yan, C. Cheng, K. Dai, C. Liu, C. Shen, Z. Guo, *J. Mater. Chem. C* **2018**, *6*, 2258; c) K. Sa, P. C. Mahakul, S. Saha, P. N. Vishwakarma, K. K. Nanda, P. Mahanandia, *Polymer Engineering & Science* **2019**, *59*, 1075.

[12] a) M. A. A. Tarawneh, R. S. Chen, S. Hj Ahmad, M. A. M. Al-Tarawni, S. A. Saraireh, *Polym. Compos.* **2019**, *40*, E695; b) D. Mondal, S. Ghorai, D. Rana, D. De, D. Chattopadhyay, *Polym. Compos.* **2019**, *40*, E1559.

[13] a) M. Zou, W. Zhao, H. Wu, H. Zhang, W. Xu, L. Yang, S. Wu, Y. Wang, Y. Chen, L. Xu, A. Cao, *Adv. Mater.* **2018**, *30*, 1704419; b) J. Lin, B. Zhong, Y. Luo, Z. Jia, D. Hu, T. Xu, D. Jia, *Polym. Compos.* **2019**, *40*, 677.

[14] a) B. Yang, X. Tang, K. Yang, F.-Z. Xuan, Y. Xiang, L. He, J. Sha, *J. Appl. Polym. Sci.* **2018**, *135*, 46263; b) S. Han, Q. Meng, X. Pan, T. Liu, S. Zhang, Y. Wang, S. Haridy, S. Araby, *J. Appl. Polym. Sci.* **2019**, *136*, 48056; c) R. Bao, S. Yan, Y. Qin, M. Lu, *J. Appl. Polym. Sci.* **2017**, *134*.

[15] a) J. Bian, G. Wang, H. L. Lin, X. Zhou, Z. J. Wang, W. Q. Xiao, X. W. Zhao, *J. Appl. Polym. Sci.* **2017**, *134*, 45055; b) S. Li, Z. Yang, J. Xu, J. Xie, *Polym. Compos.* **2018**, *39*, E2084.

[16] a) L. Valentini, S. Bittolo Bon, N. M. Pugno, *Adv. Funct. Mater.* **2017**, *27*, 1606526; b) L. Somasekharan, P. Xavier, S. Bose, A. K. Zachariah, N. Kalarikkal, S. Anil Kumar, S. Thomas, *Polym. Compos.* **2020**, *41*, 369; c) B. Bhuyan, A. Roy, S. K. Srivastava, V. Mittal, *Polymer Engineering & Science* **2018**, *58*, 1155.

[17] a) Z. Zhang, X. He, X. Wang, A. M. Rodrigues, R. Zhang, *J. Appl. Polym. Sci.* **2018**, *135*, 46091; b) X. Zhou, B. Hu, W. Q. Xiao, L. Yan, Z. J. Wang, J. J. Zhang, H. L. Lin, J. Bian, Y. Lu, *J. Appl. Polym. Sci.* **2018**, *135*, 46149; c) S. Nimanpure, S. A. R. Hashmi, R. Kumar, H. N. Bhargaw, R. Kumar, P. Nair, A. Naik, *Polym. Compos.* **2019**, *40*, 664.

[18] a) J. Li, A. I. Isayev, X. Ren, M. D. Soucek, *Polym. Int.* **2017**, *66*, 820; b) B. Chen, X. Li, X. Li, Y. Jia, J. Yang, C. Li, *Polym. Compos.* **2018**, *39*, E1626.

[19] J. Wang, C. Yan, K. J. Chee, P. S. Lee, *Adv. Mater.* **2015**, *27*, 2876.

[20] Y. Liu, K. Xu, Q. Chang, M. A. Darabi, B. Lin, W. Zhong, M. Xing, *Adv. Mater.* **2016**, *28*, 7758.

[21] S. Park, G. Thangavel, K. Parida, S. Li, P. S. Lee, *Adv. Mater.* **2019**, *31*, 1805536.

[22] S. Choi, S. I. Han, D. Jung, H. J. Hwang, C. Lim, S. Bae, O. K. Park, C. M. Tschabrunn, M. Lee, S. Y. Bae, J. W. Yu, J. H. Ryu, S.-W. Lee, K. Park, P. M. Kang, W. B. Lee, R. Nezafat, T. Hyeon, D.-H. Kim, *Nat. Nanotechnol.* **2018**, *13*, 1048.

[23] P. Bazant, I. Kuritka, O. Hudecek, M. Machovsky, M. Mrlik, T. Sedlacek, *Polym. Compos.* **2014**, *35*, 19.

[24] a) M. A. Alenizi, R. Kumar, M. Aslam, F. A. Alseroury, M. A. Barakat, *Sci. Rep.* **2019**, *9*, 12091; b) G. Bharath, S. Anwer, R. V. Mangalaraja, E. Alhseinat, F. Banat, N. Ponpandian, *Sci. Rep.* **2018**, *8*, 5718.

[25] a) S. Choi, S. I. Han, D. Kim, T. Hyeon, D.-H. Kim, *Chem. Soc. Rev.* **2019**, *48*, 1566; b) S. Yao, Y. Zhu, *Adv. Mater.* **2015**, *27*, 1480.

[26] a) C. J. Thrasher, Z. J. Farrell, N. J. Morris, C. L. Willey, C. E. Tabor, *Adv. Mater.* **2019**, *31*, 1903864; b) Y. Wang, A. Liu, Y. Han, T. Li, *Polym. Int.* **2020**, *69*, 7.

[27] D. McCoul, W. Hu, M. Gao, V. Mehta, Q. Pei, *Adv. Electron. Mater.* **2016**, *2*, 1500407.

[28] T. Q. Trung, N.-E. Lee, *Adv. Mater.* **2017**, *29*, 1603167.

[29] *Metal Filled Polymers* (Ed: S. K. Bhattacharya), CRC Press, Boca Raton, FL **1986**.

[30] Y. P. Mamunya, V. Davydenko, P. Pissis, E. Lebedev, *Eur. Polym. J.* **2002**, *38*, 1887.

[31] P. Feng, Z. Ye, Q. Wang, Z. Chen, G. Wang, X. Liu, K. Li, W. Zhao, *J. Mater. Sci.* **2020**, *55*, 8576.

[32] K. Ke, Z. Sang, I. Manas-Zloczower, *Polym. Compos.* **2020**, *41*, 468.

[33] M. Gu, W.-J. Song, J. Hong, S. Y. Kim, T. J. Shin, N. A. Kotov, S. Park, B.-S. Kim, *Sci. Adv.* **2019**, *5*, eaaw1879.

[34] N. Matsuhisa, M. Kaltenbrunner, T. Yokota, H. Jinno, K. Kuribara, T. Sekitani, T. Someya, *Nat. Commun.* **2015**, *6*, 7461.

[35] I. Kim, K. Woo, Z. Zhong, P. Ko, Y. Jang, M. Jung, J. Jo, S. Kwon, S.-H. Lee, S. Lee, H. Youn, J. Moon, *Nanoscale* **2018**, *10*, 7890.

[36] J. Wang, G. Cai, S. Li, D. Gao, J. Xiong, P. S. Lee, *Adv. Mater.* **2018**, *30*, 1706157.

[37] a) J.-E. Lim, S.-M. Lee, S.-S. Kim, T.-W. Kim, H.-W. Koo, H.-K. Kim, *Sci. Rep.* **2017**, *7*, 14685; b) W. Huang, J. Li, S. Zhao, F. Han, G. Zhang, R. Sun, C.-P. Wong, *Compos. Sci. Technol.* **2017**, *146*, 169; c) D. Son, J. Kang, O. Vardoulis, Y. Kim, N. Matsuhisa, J. Y. Oh, J. W. F. To, J. Mun, T. Katsumata, Y. Liu, A. F. McGuire, M. Krason, F. Molina-Lopez, J. Ham, U. Kraft, Y. Lee, Y. Yun, J. B. H. Tok, Z. Bao, *Nat. Nanotechnol.* **2018**, *13*, 1057; d) J. Liang, K. Tong, Q. Pei, *Adv. Mater.* **2016**, *28*, 5986.

[38] a) Y. Lin, J. Genzer, M. D. Dickey, *Adv. Sci.* **2020**, *7*, 2000192; b) N. Kazem, T. Hellebrekers, C. Majidi, *Adv. Mater.* **2017**, *29*, 1605985; c) K. Khoshmanesh, S.-Y. Tang, J. Y. Zhu, S. Schaefer, A. Mitchell, K. Kalantar-zadeh, M. D. Dickey, *Lab Chip* **2017**, *17*, 974; d) S. Yu, M. Kaviany, *J. Chem. Phys.* **2014**, *140*, 064303.

[39] a) S. Liang, Y. Li, Y. Chen, J. Yang, T. Zhu, D. Zhu, C. He, Y. Liu, S. Handschuh-Wang, X. Zhou, *J. Mater. Chem. C* **2017**, *5*, 1586; b) M. D. Dickey, *Adv. Mater.* **2017**, *29*, 1606425.

[40] a) Y. Qu, T. Nguyen-Dang, A. G. Page, W. Yan, T. Das Gupta, G. M. Rotaru, R. M. Rossi, V. D. Favrod, N. Bartolomei, F. Sorin, *Adv. Mater.* **2018**, *30*, 1707251; b) Y. Xin, H. Peng, J. Xu, J. Zhang, *Adv. Funct. Mater.* **2019**, *29*, 1808989; c) M. D. Bartlett, N. Kazem, M. J. Powell-Palm, X. Huang, W. Sun, J. A. Malen, C. Majidi, *Proc. Natl. Acad. Sci.* **2017**, *114*, 2143.

[41] M. Tavakoli, M. H. Malakooti, H. Paisana, Y. Ohm, D. Green Marques, P. Alhais Lopes, A. P. Piedade, A. T. de Almeida, C. Majidi, *Adv. Mater.* **2018**, *30*, 1801852.

[42] a) M. D. Dickey, *ACS Appl. Mater. Interfaces* **2014**, *6*, 18369; b) M. D. Dickey, R. C. Chiechi, R. J. Larsen, E. A. Weiss, D. A. Weitz, G. M. Whitesides, *Adv. Funct. Mater.* **2008**, *18*, 1097; c) P. A. Giguère, D. Lamontagne, *Science* **1954**, *120*, 390.

[43] C. Wang, K. Xia, H. Wang, X. Liang, Z. Yin, Y. Zhang, *Adv. Mater.* **2019**, *31*, 1801072.

[44] a) X. Sun, H. Sun, H. Li, H. Peng, *Adv. Mater.* **2013**, *25*, 5153; b) S. Stankovich, D. A. Dikin, G. H. Dommett, K. M. Kohlhaas, E. J. Zimney, E. A. Stach, R. D. Piner, S. T. Nguyen, R. S. Ruoff, *Nature* **2006**, *442*, 282.

[45] J. C. Huang, *Adv. Polym. Technol.* **2002**, *21*, 299.

[46] a) N. C. Das, T. K. Chaki, D. Khastgir, *Polym. Int.* **2002**, *51*, 156; b) M. Knite, V. Teteris, A. Kiploka, J. Kaupuzs, *Sens. Actuators, A* **2004**, *110*, 142.

[47] S. Chand, *J. Mater. Sci.* **2000**, *35*, 1303.

[48] a) M. T. Byrne, Y. K. Gun'ko, *Adv. Mater.* **2010**, *22*, 1672; b) X. Su, H. Li, X. Lai, Z. Chen, X. Zeng, *Adv. Funct. Mater.* **2019**, *29*, 1900554; c) Y. Song, W. Huang, C. Mu, X. Chen, Q. Zhang, A. Ran, Z. Peng, R. Sun, W. Xie, *Adv. Mater. Technol.* **2019**, *4*, 1800680.

[49] F. H. Gojny, M. H. Wichmann, B. Fiedler, I. A. Kinloch, W. Bauhofer, A. H. Windle, K. Schulte, *Polymer* **2006**, *47*, 2036.

[50] B. Wang, A. Facchetti, *Adv. Mater.* **2019**, *31*, 1901408.

[51] a) M. Javadi, Q. Gu, S. Naficy, S. Farajikhah, J. M. Crook, G. G. Wallace, S. Beirne, S. E. Moulton, *Macromol. Biosci.* **2018**, *18*, 1700270; b) M. A. A. Tarawneh, S. A. Saraireh, R. S. Chen, S. H. Ahmad, M. A. M. Al-Tarawni, M. Al-Tweissi, L. J. Yu, *J. Appl. Polym. Sci.* **2020**, *137*, 48873.

[52] Y. Wang, C. Zhu, R. Pfattner, H. Yan, L. Jin, S. Chen, F. Molina-Lopez, F. Lissel, J. Liu, N. I. Rabiah, Z. Chen, J. W. Chung, C. Linder, M. F. Toney, B. Murmann, Z. Bao, *Sci. Adv.* **2017**, *3*, e1602076.
[53] M. I. Mohd Yazid, A. F. Osman, S. A. Ghani, T. P. Leng, S. H. Mohd Din, *J. Vinyl Add. Tech.* **2018**, *24*, E186.
[54] Y.-L. Tong, B. Xu, X.-F. Du, H.-Y. Cheng, C.-F. Wang, G. Wu, S. Chen, *Macromol. Mater. Eng.* **2018**, *303*, 1700664.
[55] Y. D. Suh, J. Jung, H. Lee, J. Yeo, S. Hong, P. Lee, D. Lee, S. H. Ko, *J. Mater. Chem. C* **2017**, *5*, 791.
[56] M. D. Ho, Y. Ling, L. W. Yap, Y. Wang, D. Dong, Y. Zhao, W. Cheng, *Adv. Funct. Mater.* **2017**, *27*, 1700845.
[57] X. Cauchy, J.-E. Klemberg-Sapieha, D. Therriault, *Adv. Eng. Mater.* **2018**, *20*, 1800541.
[58] S. Dhote, K. Behdinan, J. Andrysek, J. Bian, *J. Compos. Mater.* **2019**, *0*, 0021998319890406.
[59] I. C. Kim, T.-H. Kim, S. H. Lee, B.-S. Kim, *Sci. Rep.* **2018**, *8*, 11517.
[60] S. Park, K. Mondal, R. M. Treadway III, V. Kumar, S. Ma, J. D. Holbery, M. D. Dickey, *ACS Appl. Mater. Interfaces* **2018**, *10*, 11261.
[61] J.-Y. Sun, X. Zhao, W. R. K. Illeperuma, O. Chaudhuri, K. H. Oh, D. J. Mooney, J. J. Vlassak, Z. Suo, *Nature* **2012**, *489*, 133.
[62] a) E. Nilsson, H. Oxfall, W. Wandelt, R. Rychwalski, B. Hagström, *J. Appl. Polym. Sci.* **2013**, *130*, 2579; b) Y. Kim, J. Zhu, B. Yeom, M. Di Prima, X. Su, J.-G. Kim, S. J. Yoo, C. Uher, N. A. Kotov, *Nature* **2013**, *500*, 59; c) I. Brook, G. Mechrez, R. Y. Suckeveriene, R. Tchoudakov, S. Lupo, M. Narkis, *Polym. Compos.* **2014**, *35*, 788.
[63] S. Leyva Egurrola, T. del Castillo Castro, M. M. Castillo Ortega, J. C. Encinas, P. J. Herrera Franco, J. Bonilla Cruz, T. E. Lara Ceniceros, *J. Appl. Polym. Sci.* **2017**, *134*.
[64] S. Lee, A. Reuveny, J. Reeder, S. Lee, H. Jin, Q. Liu, T. Yokota, T. Sekitani, T. Isoyama, Y. Abe, Z. Suo, T. Someya, *Nat. Nanotechnol.* **2016**, *11*, 472.
[65] W.-J. Song, J. Park, D. H. Kim, S. Bae, M.-J. Kwak, M. Shin, S. Kim, S. Choi, J.-H. Jang, T. J. Shin, S. Y. Kim, K. Seo, S. Park, *Adv. Energy Mater.* **2018**, *8*, 1702478.
[66] H. R. Gholshan Tafti, P. Valipour, M. Mirjalili, *Polym. Compos.* **2018**, *39*, E2298.
[67] I. Brook, R. Tchoudakov, R. Y. Suckeveriene, M. Narkis, *Polym. Adv. Technol.* **2015**, *26*, 889.
[68] a) A. Shayesteh Zeraati, U. Sundararaj, *Can. J. Chem. Eng.* **2020**, *98*, 1036; b) J.-Z. Liang, *Polym. Compos.* **2019**, *40*, E1801; c) D. P. Schmitz, T. I. Silva, S. D. A. S. Ramoa, G. M. O. Barra, A. Pegoretti, B. G. Soares, *J. Appl. Polym. Sci.* **2018**, *135*, 46546.
[69] J. Y. Woo, K. K. Kim, J. Lee, J. T. Kim, C.-S. Han, *Nanotechnology* **2014**, *25*, 285203.
[70] Y. Ding, T. Xu, O. Onyilagha, H. Fong, Z. Zhu, *ACS Appl. Mater. Interfaces* **2019**, *11*, 6685.
[71] P. Lv, K. Yu, X. Tan, R. Zheng, Y. Ni, Z. Wang, C. Liu, W. Wei, *RSC Adv.* **2016**, *6*, 11256.
[72] Y. Tang, S. Gong, Y. Chen, L. W. Yap, W. Cheng, *ACS Nano* **2014**, *8*, 5707.
[73] a) J. Zhou, H. Li, R. Tian, R. Dugnani, H. Lu, Y. Chen, Y. Guo, H. Duan, H. Liu, *Sci. Rep.* **2017**, *7*, 5535; b) J. Jeddi, A. A. Katbab, *Polym. Compos.* **2018**, *39*, 3452.
[74] S. Lee, S. Shin, S. Lee, J. Seo, J. Lee, S. Son, H. J. Cho, H. Algadi, S. Al-Sayari, D. E. Kim, T. Lee, *Adv. Funct. Mater.* **2015**, *25*, 3114.
[75] J. Shi, X. Li, H. Cheng, Z. Liu, L. Zhao, T. Yang, Z. Dai, Z. Cheng, E. Shi, L. Yang, Z. Zhang, A. Cao, H. Zhu, Y. Fang, *Adv. Funct. Mater.* **2016**, *26*, 2078.
[76] a) Z. F. Liu, S. Fang, F. A. Moura, J. N. Ding, N. Jiang, J. Di, M. Zhang, X. Lepró, D. S. Galvão, C. S. Haines, N. Y. Yuan, S. G. Yin, D. W. Lee, R. Wang, H. Y. Wang, W. Lv, C. Dong, R. C. Zhang, M. J. Chen, Q. Yin, Y. T. Chong, R. Zhang, X. Wang, M. D. Lima, R. Ovalle-Robles, D. Qian, H. Lu, R. H. Baughman, *Science* **2015**, *349*, 400; b) D. J. Lipomi, M. Vosgueritchian, B. C. K. Tee, S. L. Hellstrom, J. A. Lee, C. H. Fox, Z. Bao, *Nat. Nanotechnol.* **2011**, *6*, 788.
[77] B. W. An, B. G. Hyun, S.-Y. Kim, M. Kim, M.-S. Lee, K. Lee, J. B. Koo, H. Y. Chu, B.-S. Bae, J.-U. Park, *Nano Lett.* **2014**, *14*, 6322.
[78] C. M. Ajmal, M. M. Menamparambath, H. R. Choi, S. Baik, *Nanotechnology* **2016**, *27*, 225603.
[79] F. Zhang, S. Wu, S. Peng, Z. Sha, C. H. Wang, *Compos. Sci. Technol.* **2019**, *172*, 7.
[80] Y. Z. Yoo, J.-Y. Na, Y. S. Choi, Y. J. Lim, J.-H. Kim, Y.-B. Kim, J.-H. Kim, S.-K. Kim, T.-Y. Seong, *Small* **2018**, *14*, 1800056.
[81] a) A. Aliprandi, T. Moreira, C. Anichini, M.-A. Stoeckel, M. Eredia, U. Sassi, M. Bruna, C. Pinheiro, C. A. T. Laia, S. Bonacchi, P. Samorì, *Adv. Mater.* **2017**, *29*, 1703225; b) P. Cataldi, I. S. Bayer, F. Bonaccorso, V. Pellegrini, A. Athanassiou, R. Cingolani, *Adv. Electron. Mater.* **2015**, *1*, 1500224.
[82] F.-J. Lin, C. Guo, W.-T. Chuang, C.-L. Wang, Q. Wang, H. Liu, C.-S. Hsu, L. Jiang, *Adv. Mater.* **2017**, *29*, 1606987.
[83] Q. Wang, S. Ling, X. Liang, H. Wang, H. Lu, Y. Zhang, *Adv. Funct. Mater.* **2019**, *29*, 1808695.
[84] J. E. Q. Quinsaat, I. Burda, R. Krämer, D. Häfliger, F. A. Nüesch, M. Dascalu, D. M. Opris, *Sci. Rep.* **2019**, *9*, 13331.
[85] a) H. Lee, T. K. Choi, Y. B. Lee, H. R. Cho, R. Ghaffari, L. Wang, H. J. Choi, T. D. Chung, N. Lu, T. Hyeon, S. H. Choi, D.-H. Kim, *Nat. Nanotechnol.* **2016**, *11*, 566; b) A. D. Valentine, T. A. Busbee, J. W. Boley, J. R. Raney, A. Chortos, A. Kotikian, J. D. Berrigan, M. F. Durstock, J. A. Lewis, *Adv. Mater.* **2017**, *29*, 1703817.
[86] Y. Kang, G. Wang, S. Zhao, J. Li, L. Di, Y. Feng, J. Yin, J. Zhu, *Small* **2020**, 2004793.
[87] J. Lee, B. Llerena Zambrano, J. Woo, K. Yoon, T. Lee, *Adv. Mater.* **2020**, *32*, 1902532.
[88] Y. Lee, S. Bae, B. Hwang, M. Schroeder, Y. Lee, S. Baik, *J. Mater. Chem. C* **2019**, *7*, 12297.
[89] J. T. Han, J. I. Jang, J. Y. Cho, J. Y. Hwang, J. S. Woo, H. J. Jeong, S. Y. Jeong, S. H. Seo, G.-W. Lee, *Sci. Rep.* **2017**, *7*, 4931.
[90] D. Esrafilzadeh, R. Jalili, E. M. Stewart, S. H. Aboutalebi, J. M. Razal, S. E. Moulton, G. G. Wallace, *Adv. Funct. Mater.* **2016**, *26*, 3105.
[91] J. Zhou, X. Xu, Y. Xin, G. Lubineau, *Adv. Funct. Mater.* **2018**, *28*, 1705591.
[92] Y. Zhao, D. Dong, S. Gong, L. Brassart, Y. Wang, T. An, W. Cheng, *Adv. Electron. Mater.* **2019**, *5*, 1800462.
[93] F. Pierini, M. Lanzi, P. Nakielski, S. Pawłowska, K. Zembrzycki, T. A. Kowalewski, *Polym. Adv. Technol.* **2016**, *27*, 1465.
[94] B. Zhang, W. Li, M. Nogi, C. Chen, Y. Yang, T. Sugahara, H. Koga, K. Suganuma, *ACS Appl. Mater. Interfaces* **2019**, *11*, 18540.
[95] Y. Wang, L. Zhang, D. Wang, *Adv. Mater. Technol.* **2019**, *4*, 1900721.
[96] S. Peng, S. Wu, F. Zhang, C. H. Wang, *Adv. Mater. Technol.* **2019**, *4*, 1900060.
[97] Y. Cai, J. Shen, Z. Dai, X. Zang, Q. Dong, G. Guan, L.-J. Li, W. Huang, X. Dong, *Adv. Mater.* **2017**, *29*, 1606411.
[98] J. Tolvanen, J. Hannu, H. Jantunen, *Sci. Rep.* **2018**, *8*, 13241.
[99] J. M. Kim, Y. Lee, M. G. Jang, C. Han, W. N. Kim, *J. Appl. Polym. Sci.* **2017**, *134*.
[100] R. Guo, X. Sun, B. Yuan, H. Wang, J. Liu, *Adv. Sci.* **2019**, *6*, 1901478.
[101] J. Kim, W. Kim, G. Jang, D. S. Hyeon, M. H. Park, J. P. Hong, *Adv. Energy Mater.* **2020**, *10*, 1903217.
[102] K. Sim, Z. Rao, H.-J. Kim, A. Thukral, H. Shim, C. Yu, *Sci. Adv.* **2019**, *5*, eaav5749.
[103] G. Yun, S.-Y. Tang, S. Sun, D. Yuan, Q. Zhao, L. Deng, S. Yan, H. Du, M. D. Dickey, W. Li, *Nat. Commun.* **2019**, *10*, 1300.

[104] K.-Y. Chun, Y. Oh, J. Rho, J.-H. Ahn, Y.-J. Kim, H. R. Choi, S. Baik, *Nat. Nanotechnol.* **2010**, *5*, 853.
[105] J. Feng, H. Xia, F. You, H. Mao, X. Ma, H. Tao, X. Zhao, M.-C. Wang, *J. Alloys Compd.* **2018**, *735*, 607.
[106] H. Hu, M. Pauly, O. Felix, G. Decher, *Nanoscale* **2017**, *9*, 1307.
[107] L. Meng, R. Bian, C. Guo, B. Xu, H. Liu, L. Jiang, *Adv. Mater.* **2018**, *30*, 1706938.
[108] H. Hu, S. Wang, S. Wang, G. Liu, T. Cao, Y. Long, *Adv. Funct. Mater.* **2019**, *29*, 1902922.
[109] a) G. Yun, S.-Y. Tang, Q. Zhao, Y. Zhang, H. Lu, D. Yuan, S. Sun, L. Deng, M. D. Dickey, W. Li, *Matter* **2020**, *3*, 824; b) C. Sui, Y. Yang, R. J. Headrick, Z. Pan, J. Wu, J. Zhang, S. Jia, X. Li, W. Gao, O. S. Dewey, C. Wang, X. He, J. Kono, M. Pasquali, J. Lou, *Nanoscale* **2018**, *10*, 14938.
[110] H. Chen, Y. Jing, J.-H. Lee, D. Liu, J. Kim, S. Chen, K. Huang, X. Shen, Q. Zheng, J. Yang, S. Jeon, J.-K. Kim, *Mater. Horiz.* **2020**, *7*, 2378.
[111] S. Shang, W. Zeng, X.-M. Tao, *J. Mater. Chem.* **2011**, *21*, 7274.
[112] Y. Zhang, C. J. Sheehan, J. Zhai, G. Zou, H. Luo, J. Xiong, Y. T. Zhu, Q. X. Jia, *Adv. Mater.* **2010**, *22*, 3027.
[113] F. Xu, X. Wang, Y. Zhu, Y. Zhu, *Adv. Funct. Mater.* **2012**, *22*, 1279.
[114] J. Li, S. Qi, J. Liang, L. Li, Y. Xiong, W. Hu, Q. Pei, *ACS Appl. Mater. Interfaces* **2015**, *7*, 14140.
[115] Y. Zhu, F. Xu, *Adv. Mater.* **2012**, *24*, 1073.
[116] a) J. Park, I. You, T. Y. Kim, J. Song, U. Jeong, *Nanotechnology* **2019**, *30*, 315502; b) Y. Won, A. Kim, W. Yang, S. Jeong, J. Moon, *NPG Asia Mater.* **2014**, *6*, e132; c) P. Lee, J. Lee, H. Lee, J. Yeo, S. Hong, K. H. Nam, D. Lee, S. S. Lee, S. H. Ko, *Adv. Mater.* **2012**, *24*, 3326; d) F. Xu, Y. Zhu, *Adv. Mater.* **2012**, *24*, 5117.
[117] A. Hirsch, H. O. Michaud, A. P. Gerratt, S. de Mulatier, S. P. Lacour, *Adv. Mater.* **2016**, *28*, 4507.
[118] P. Song, H. Qin, H.-L. Gao, H.-P. Cong, S.-H. Yu, *Nat. Commun.* **2018**, *9*, 2786.
[119] M. Park, J. Im, M. Shin, Y. Min, J. Park, H. Cho, S. Park, M.-B. Shim, S. Jeon, D.-Y. Chung, J. Bae, J. Park, U. Jeong, K. Kim, *Nat. Nanotechnol.* **2012**, *7*, 803.
[120] X. Bai, S. Liao, Y. Huang, J. Song, Z. Liu, M. Fang, C. Xu, Y. Cui, H. Wu, *Nano Lett.* **2017**, *17*, 1883.
[121] a) S. P. Lacour, D. Chan, S. Wagner, T. Li, Z. Suo, *Appl. Phys. Lett.* **2006**, *88*, 204103; b) I. M. Graz, D. P. J. Cotton, S. P. Lacour, *Appl. Phys. Lett.* **2009**, *94*, 071902.
[122] X. Li, X. Ruan, W. Yao, L. Liu, B. Tian, H. Wang, Y. Feng, R. Xia, W. Wu, *Sci. China Mater.* **2019**, *62*, 1412.
[123] K. L. Lin, J. Chae, K. Jain, *IEEE Trans. Adv. Packag.* **2010**, *33*, 592.
[124] D. Stauffer, A. Aharony, in *Introduction to Percolation Theory*, Taylor & Francis, London **1992**.
[125] a) J. Li, P. C. Ma, W. S. Chow, C. K. To, B. Z. Tang, J.-K. Kim, *Adv. Funct. Mater.* **2007**, *17*, 3207; b) J. Li, J.-K. Kim, *Compos. Sci. Technol.* **2007**, *67*, 2114.
[126] M. Weber, M. R. Kamal, *Polym. Compos.* **1997**, *18*, 711.
[127] W. Bauhofer, J. Z. Kovacs, *Compos. Sci. Technol.* **2009**, *69*, 1486.
[128] K. Dai, X.-B. Xu, Z.-M. Li, *Polymer* **2007**, *48*, 849.
[129] a) P. J. Brigandi, D. Carolan, J. M. Cogen, R. A. Pearson, *J. Appl. Polym. Sci.* **2017**, *134*; b) A. Paydayesh, F. Pashaei Soorbaghi, A. Aref Azar, A. Jalali-Arani, *Polym. Compos.* **2019**, *40*, 704; c) D. S. McLachlan, M. Blaszkiewicz, R. E. Newnham, *J. Am. Ceram. Soc.* **1990**, *73*, 2187; d) M. Wang, R. Gurunathan, K. Imasato, N. R. Geisendorfer, A. E. Jakus, J. Peng, R. N. Shah, M. Grayson, G. J. Snyder, *Adv. Theory Simul.* **2019**, *2*, 1800125.
[130] H. Yao, Y.-P. Hsieh, J. Kong, M. Hofmann, *Nat. Mater.* **2020**, *19*, 745.
[131] X. Ni, C. Hui, N. Su, W. Jiang, F. Liu, *Nanotechnology* **2018**, *29*, 075401.
[132] Y. Lu, H. Wu, J. Liu, Y. Liu, J. Zhao, P. Liu, J. Wang, H. Liang, Y. Huang, A. Song, *J. Appl. Polym. Sci.* **2019**, *136*, 48222.
[133] S.-H. Park, J. Hwang, G.-S. Park, J.-H. Ha, M. Zhang, D. Kim, D.-J. Yun, S. Lee, S. H. Lee, *Nat. Commun.* **2019**, *10*, 2537.
[134] T. Ding, L. Wang, P. Wang, *J. Polym. Sci., Part B: Polym. Phys.* **2007**, *45*, 2700.
[135] T. C. Theodosiou, D. A. Saravanos, *Compos. Sci. Technol.* **2010**, *70*, 1312.
[136] N. Hu, Y. Karube, M. Arai, T. Watanabe, C. Yan, Y. Li, Y. Liu, H. Fukunaga, *Carbon* **2010**, *48*, 680.
[137] M. Jian, K. Xia, Q. Wang, Z. Yin, H. Wang, C. Wang, H. Xie, M. Zhang, Y. Zhang, *Adv. Funct. Mater.* **2017**, *27*, 1606066.
[138] M. Amjadi, M. Sitti, *Adv. Sci.* **2018**, *5*, 1800239.
[139] J. Hwang, H. Sohn, S. H. Lee, *Sci. Rep.* **2018**, *8*, 16617.
[140] X. Li, H. Hu, T. Hua, B. Xu, S. Jiang, *Nano Res.* **2018**, *11*, 5799.
[141] K. Yamaguchi, J. J. C. Busfield, A. G. Thomas, *J. Polym. Sci., Part B: Polym. Phys.* **2003**, *41*, 2079.
[142] Z. Tang, S. Jia, C. Zhou, B. Li, *ACS Appl. Mater. Interfaces* **2020**, *12*, 28669.
[143] a) L. Chen, G. H. Chen, L. Lu, *Adv. Funct. Mater.* **2007**, *17*, 898; b) J. Hwang, J. Jang, K. Hong, K. N. Kim, J. H. Han, K. Shin, C. E. Park, *Carbon* **2011**, *49*, 106.
[144] J.-W. Zha, W. Huang, S.-J. Wang, D.-L. Zhang, R. K. Y. Li, Z.-M. Dang, *Adv. Mater. Interfaces* **2016**, *3*, 1500418.
[145] R. V. Salvatierra, C. E. Cava, L. S. Roman, A. J. G. Zarbin, *Adv. Funct. Mater.* **2013**, *23*, 1490.
[146] J. Jones, S. P. Lacour, S. Wagner, Z. Suo, *J. Vac. Sci. Technol. A* **2004**, *22*, 1723.
[147] H. Wang, Y. Yao, Z. He, W. Rao, L. Hu, S. Chen, J. Lin, J. Gao, P. Zhang, X. Sun, X. Wang, Y. Cui, Q. Wang, S. Dong, G. Chen, J. Liu, *Adv. Mater.* **2019**, *31*, 1901337.
[148] M.-S. Lee, K. Lee, S.-Y. Kim, H. Lee, J. Park, K.-H. Choi, H.-K. Kim, D.-G. Kim, D.-Y. Lee, S. Nam, J.-U. Park, *Nano Lett.* **2013**, *13*, 2814.
[149] S. Stassi, G. Canavese, *J. Polym. Sci., Part B: Polym. Phys.* **2012**, *50*, 984.
[150] B. Han, Y. Wang, S. Sun, X. Yu, J. Ou, *Composites A* **2014**, *59*, 105.
[151] D. Lee, H. Lee, Y. Jeong, Y. Ahn, G. Nam, Y. Lee, *Adv. Mater.* **2016**, *28*, 9364.
[152] D. Bloor, K. Donnelly, P. J. Hands, P. Laughlin, D. Lussey, *J. Phys. D: Appl. Phys.* **2005**, *38*, 2851.
[153] H. A. K. Toprakci, S. K. Kalanadhabhatla, R. J. Spontak, T. K. Ghosh, *Adv. Funct. Mater.* **2013**, *23*, 5536.
[154] C. Lim, Y. Shin, J. Jung, J. H. Kim, S. Lee, D.-H. Kim, *APL Mater.* **2019**, *7*, 031502.
[155] X. Wu, Y. Han, X. Zhang, Z. Zhou, C. Lu, *Adv. Funct. Mater.* **2016**, *26*, 6246.
[156] a) C. B. Cooper, K. Arutselvan, Y. Liu, D. Armstrong, Y. Lin, M. R. Khan, J. Genzer, M. D. Dickey, *Adv. Funct. Mater.* **2017**, *27*, 1605630; b) S. Chen, Z. Lou, D. Chen, K. Jiang, G. Shen, *Adv. Mater. Technol.* **2016**, *1*, 1600136.
[157] a) Y. Wei, S. Chen, Y. Lin, Z. Yang, L. Liu, *J. Mater. Chem. C* **2015**, *3*, 9594; b) T. Dinh, T. Nguyen, H.-P. Phan, N.-T. Nguyen, D. V. Dao, J. Bell, *Biosens. Bioelectron.* **2020**, *166*, 112460.
[158] J. Yang, D. Tang, J. Ao, T. Ghosh, T. V. Neumann, D. Zhang, E. Piskarev, T. Yu, V. K. Truong, K. Xie, Y.-C. Lai, Y. Li, M. D. Dickey, *Adv. Funct. Mater.* **2020**, *30*, 2002611.
[159] Z. Chen, P.-C. Hsu, J. Lopez, Y. Li, J. W. F. To, N. Liu, C. Wang, Sean C. Andrews, J. Liu, Y. Cui, Z. Bao, *Nat. Energy* **2016**, *1*, 15009.
[160] a) T. Xu, Y. Ding, Z. Wang, Y. Zhao, W. Wu, H. Fong, Z. Zhu, *J. Mater. Chem. C* **2017**, *5*, 10288; b) Y. Ma, Y. Yue, H. Zhang, F. Cheng, W. Zhao, J. Rao, S. Luo, J. Wang, X. Jiang, Z. Liu, N. Liu, Y. Gao, *ACS Nano* **2018**, *12*, 3209.
[161] S. Li, W. Li, J. Nie, D. Liu, G. Sui, *Carbon* **2019**, *143*, 154.

[162] Y. Yan, H. Xia, Y. Qiu, Z. Xu, Q.-Q. Ni, *Phys. Status Solidi A* **2019**, *216*, 1900663.
[163] S. Lin, Y. Zhong, X. Zhao, T. Sawada, X. Li, W. Lei, M. Wang, T. Serizawa, H. Zhu, *Adv. Mater.* **2018**, *30*, 1803004.
[164] F. Krisnadi, L. L. Nguyen, J. Ankit, *Adv. Mater.* **2020**, *32*, 2001642.
[165] Q. Zhang, Y. Zhang, Z. Meng, W. Tong, X. Yu, Q. An, *Sci. Rep.* **2017**, *7*, 12296.
[166] C. Tondera, T. F. Akbar, A. K. Thomas, W. Lin, C. Werner, V. Busskamp, Y. Zhang, I. R. Minev, *Small* **2019**, *15*, 1901406.
[167] N. Luo, Y. Huang, J. Liu, S.-C. Chen, C. P. Wong, N. Zhao, *Adv. Mater.* **2017**, *29*, 1702675.
[168] Y. Yoon, K. Samanta, H. Lee, K. Lee, A. P. Tiwari, J. Lee, J. Yang, H. Lee, *Sci. Rep.* **2015**, *5*, 14177.

Guolin Yun received his B.S. in Theoretical and Applied Mechanics in 2017 from the University of Science and Technology of China (USTC, China). He is currently a Ph.D. student at the University of Wollongong (UOW, Australia) under the guidance of Professor Weihua Li. His research focus is on the liquid metal-filled hybrid conductive composites and their applications in flexible sensors and stretchable electronics.

Shiyang Tang currently is a lecturer (assistant professor) in the Department of Electronic, Electrical and Systems Engineering at the University of Birmingham, UK. He received his B.Eng. (first-class honours) in Electrical Engineering and Ph.D. in Microelectromechanical Systems (MEMS) from the RMIT University, Australia, in 2012 and 2015, respectively. He was the recipient of the Discovery Early Career Researcher Award from the Australian Research Council and the vice chancellor's postdoctoral research fellow from the University of Wollongong, Australia. His research interests include developing microfluidic platforms for biomedical studies and liquid metal-enabled micro-/nanoscale platforms.

Michael D. Dickey received a B.S. in Chemical Engineering from Georgia Institute of Technology (1999) and a Ph.D. in Chemical Engineering from the University of Texas at Austin (2006) under the guidance of Professor Grant Willson. From 2006 to 2008, he was a postdoctoral fellow in the lab of Professor George Whitesides at Harvard University. In 2008, he joined the Department of Chemical & Biomolecular Engineering at North Carolina State University, where he is currently the alcoa professor. Michael's research interests include patterning and actuating soft materials by studying and harnessing thin films, interfaces, and unconventional fabrication techniques.

Weihua Li received his B.Eng. (1992) and M.Eng. (1995) at University of Science and Technology of China and Ph.D. (2001) at Nanyang Technological University (NTU). From 2001 to 2003, he was with the School of Mechanical and Aerospace Engineering of NTU as a research associate/fellow. In 2003, he joined the School of Mechanical, Materials, Mechatronic and Biomedical Engineering at the University of Wollongong, where he is currently a senior professor and academic program director for Mechatronic Engineering. His research focuses on smart materials and structures, dynamics and vibration control, microfluidics, lab on a chip, and vehicle technology.